Pattern formation in laser-induced melting

Chuck Yeung and Rashmi C. Desai
Department of Physics, University of Toronto, Toronto, Ontario, Canada M5S 1A7
(Received 18 October 1993)

A laser focused onto a semiconductor film can create a disordered lamellae pattern of coexisting molten-solid regions. We present a continuum model based on the higher reflectivity of the molten regions. For a large latent heat, this model becomes equivalent to a dynamical model of block copolymers. The characteristic wave number of the lamellae is the one marginally stable to slow variations in the orientation (the zigzag instability) and can be obtained via systematic expansions from two limits. The lamellae can also become unstable to the zigzag instability and Eckhaus instability (slow variations in the wave number) simultaneously. This instability is a signal of dynamic steady states. We numerically study the behavior after a quench. The lamellar size is in agreement with the analytic results and with experiments. For shallow quenches, locally parallel stripes slowly straighten out in time. For deep quenches, a disordered lamellar structure is created. We construct the director field and determine the orientational correlation length. Near onset, the correlation is fixed by the system size. Far from onset, the correlation length saturates at a finite value. We study the transition to the time-dependent asymptotic states as the latent heat is decreased.

PACS number(s): 47.54.+r, 44.30.+v, 05.70.Ln, 78.66.−w

I. INTRODUCTION

A laser focused onto a semiconductor film such as silicon can induce melting. At low laser intensity the incident light will simply raise the sample temperature. At large laser intensity a uniform molten surface will be created. However, the laser intensity can be adjusted so that melting is initiated but molten and solid regions coexist [1–6]. Therefore the area onto which the laser is directed contains both molten and solid regions of size much smaller than the diameter of the illuminated area.

The coexisting molten-solid regions can arise from two different mechanisms. One possibility discussed by Preston *et al.* [4,7] is that, due to the coherence of the laser beam, there can be interference between the incident and surface scattered fields. This leads to spatially periodic power deposition and solid-melt patterns that depend on the wavelength and orientation of the incident light [3,4].

In this paper we will be interested in a second mechanism. It was conjectured that the nonuniformity can be due to the increased reflectivity of the molten regions [2,8]. Following the argument of Hawkins and Biegelsen [2], assume that laser energy flux J_1 is required to raise the solid sample to the melting temperature. Due to the higher reflectivity, the energy flux J_2 required to maintain a homogeneous molten phase at the melting temperature will be much higher. Therefore for energy fluxes between J_1 and J_2 a homogeneous phase is not possible. Instead a heterogeneous surface is created in which the molten regions are undercooled and the solid regions superheated. Although a free energy argument may not be justified for the nonequilibrium steady state, Hawkins and Biegelsen [2] balanced the surface energy due to the solid-liquid interfaces with the increase in the free energy due to the undercooling (superheating) of the melt (solid) phase to relate the wavelength of the patterns to the average undercooling. Jackson and Kurtze [8], on the other hand, studied the stability of a periodic array of solid and molten stripes using a phenomenological interface description. They found that, if the wavelength of the pattern is within a specific band, the pattern is stable to infinitesimal perturbations of the orientation of the stripes. This thermally controlled regime has also been observed experimentally and is characterized by a disordered lamellar structure [2,6].

In addition to static patterns, the transition between the parallel stripes and disordered lamellar phases have been studied. It was found that the transition was reversible but displays hysteresis characteristic of a first order transition [6]. Dynamical structures have also been observed [1–4] in which the patterns are not static but evolves to some, possibly chaotic, time-dependent asymptotic state.

In Sec. II we discuss our continuum model of laser induced melting. The dynamics are given by a set of coupled partial differential equations for the order parameter and temperature field. The effect of the incoming energy of the laser, the heat flow to the substrate, and the order-parameter-dependent reflectivity are included in the dynamics. In Sec. III we show that, in the limit of large latent heat, this model is equivalent to a model of block copolymers [9,10]. In particular the static solutions are always the same as that of block copolymers. Using the analogy with block copolymers the characteristic length scale of the patterns is the one that minimizes the free energy. We show that this length scale can be obtained via systematic expansions close to (weak segregation) and far away (strong segregation) from onset (the parameters where pattern formation first occurs). These regimes are characterized by different dependence on the control parameter [10–12] and by qualitatively different

patterns. Near onset, locally parallel stripes are observed while, far from onset, disordered lamellar structures are found.

Although we discuss a specific model, this analogy between seemingly unrelated systems leads us to expect that most of our results should be relevant to many systems which favor phase separation at short length scales but has a mechanism suppressing macroscopic phase separation. Examples include ferrofluids [13], ferromagnets [14], and monolayer films [15,16] as well as Raleigh-Bénard convection [17]. In particular, the patterns after a quench are characterized by two length scales corresponding to the characteristic length of the local domains (stripes for the symmetric case) and the length on which the orientation of the domains are correlated. This additional length scale has been suggested for Raleigh-Bénard convection [18,19].

Whereas for large latent heat the dynamics are equivalent to that of block copolymers, for other parameters the static state is never reached and the system instead settles into a time-dependent asymptotic state. In Sec. IV we discuss different stability criteria. We consider the linear analysis of the homogeneous state. We derive the phase diffusion equations [20,21] describing the slowly varying lamellae. Using the phase diffusion equations we reobtain the equilibrium length scale using the rigourous criteria that the selected length scale is the one marginally stable to the zigzag instability (i.e., marginally stable to slow variations in the orientation of the stripes). We therefore make concrete, and relate to one another, the seemingly unrelated free energy [2] and interfacial stability approaches [8].

In addition, we find that a new instability is possible in which the lamellae become unstable to both the Eckhaus and zigzag instability simultaneously. This instability occurs at small latent heat and marks the limit of metastability of the parallel lamellae. We conjecture that this instability signals the presence of the time-dependent asymptotic states which have also been observed experimentally [1,2,6].

In Sec. V we present a numerical study. First we consider the static steady state. Previous simulations have only been able to probe close to onset [12,22]. Here we find agreement near and far from onset. To study the correlation between the orientation of stripes, we construct a director field pointing in the direction of the stripes. Near onset, the orientational correlation length is much larger (possibly only limited by the system size) than the pattern wavelength. This leads to the large regions of locally parallel stripes. Far from onset, the orientational correlation length is of the same order as the pattern wavelength. A disordered lamellae is formed in which the lamellae bend on the same length scale as the lamellar width. The ratio of the correlation length divided by the pattern wavelength decreases monotonically as a function of the quench depth. We speculate that a nonequilibrium Kosterlitz-Thouless-like transition separating regimes with long range orientational order from regimes without. We then map out the phase boundary between static and time-dependent asymptotic states. We demonstrate that the various regimes are described by the phase diffusion dynamics and not by the linear dynamics around the unstable initial condition.

II. MODEL EQUATIONS

We introduce our model of laser induced melting. Let ϕ be a dimensionless order parameter field which characterises the solid or liquid phases. At coexistence we choose $\phi = 1$ for the liquid phase and $\phi = -1$ for the solid phase. The free energy is

$$F\{\phi\} = \int d\mathbf{r} \left[\rho_0 \epsilon_0 \left(f(\phi) + \frac{\xi_0^2}{2} |\nabla \phi|^2 \right) - \rho_0 \frac{L}{2} u \phi \right]. \tag{2.1}$$

Since there are two coexisting phases, $f(\phi)$ is required to be a dimensionless function of double well form with minima at $\phi = \pm 1$ corresponding to the liquid and solid phases. For simplicity we also assume $f(\phi)$ to be symmetric. The $|\nabla \phi|^2$ term penalizes gradients in ϕ and is required since, in the absence of driving, the homogeneous state has the lowest free energy. The last term is the coupling to the reduced temperature $u = (T - T_m)/T_m$, where T_m is the melting temperature. For $u > 0$, the liquid phase is favored while for $u < 0$ the solid phase has the lower free energy. The physical constants are as follows (for simplicity we assume the two phases are symmetric): ρ_0 is the mass per unit volume, ϵ_0 is a constant with units of energy/mass, ξ_0 is a microscopic interfacial width, and L is the latent heat per unit mass. The surface tension is $\sigma = \rho_0 \epsilon_0 \xi_0 \bar{\sigma}$, where the dimensionless surface tension $\bar{\sigma}$ depends on the precise form of $f(\phi)$ and is of order unity. For $f(\phi) = -\phi^2/2 + \phi^4/4$, $\bar{\sigma} = 2\sqrt{2}/3$.

To describe the dynamics of ϕ we assume that ϕ obeys the time-dependent Ginzburg-Landau equation

$$\begin{aligned} \partial_t \phi(\mathbf{r},t) &= -\frac{1}{\rho_0 \epsilon_0 \tau_0} \frac{\delta F}{\delta \phi(\mathbf{r},t)} \\ &= \frac{1}{\tau_0} \left[-\mu_B(\phi(\mathbf{r},t)) + \xi_0^2 \nabla^2 \phi(\mathbf{r},t) \right. \\ &\quad \left. + \frac{L}{2\epsilon_0} u(\mathbf{r},t) \right], \end{aligned} \tag{2.2}$$

where $\mu_B = \partial f/\partial \phi$ and τ_0 is a microscopic time scale.

We also need the dynamics of the reduced temperature field u. In actual experiments the geometry is not translationally invariant [1–6]. Here we consider a simpler geometry in which the film sits on a substrate which, in turn, is attached to a heat bath. The thickness of the film is assumed sufficiently small so that all variation in perpendicular direction can be neglected. (This will be true if the thermal conductivity of the substrate is much smaller than that of the film.) The reduced temperature field obeys

$$\rho_0 C_p\, \partial_t u = K_T \nabla^2 u - \frac{\rho_0 L}{2T_m}\, \partial_t \phi$$

$$+ \frac{1}{hT_m} J_{\rm in}(\phi) - \frac{1}{hT_m} J_{\rm out}(u). \qquad (2.3)$$

Here K_T is the thermal conductivity, C_p the specific heat per unit mass, and h the thickness of the film.

The incoming flux is $J_{\rm in}(\phi) = J_0[1 - R(\phi)]$, where J_0 is the energy flux of the laser and $R(\phi)$ is the reflectivity which is higher in the molten phase. For simplicity we assume that $R(\phi)$ is linear in ϕ. We write $J_{\rm in}$ as

$$J_{\rm in}(\phi) = J_{\rm in}(\phi = 0) - J_0 \frac{\Delta R}{2} \phi, \qquad (2.4)$$

where ΔR is the difference in the reflectivity between the solid and melt phases.

The outgoing flux is $J_{\rm out}(T) = (K_s/d)\,(T - T_0)$, where K_s is the thermal conductivity of the substrate, d is some length of the order of the substrate thickness, and $T_0 < T_m$ is the temperature at the heat sink. We assume that the system is maintained close to the melting temperature so the dependence of the outgoing flux on the local temperature can be neglected. The net flux is then

$$J_{\rm total} = J_{\rm in}(\phi) - J_{\rm out}(T) = \Delta J - J_0 \frac{\Delta R}{2} \phi, \qquad (2.5)$$

where $\Delta J \equiv J_{\rm in}(\phi = 0) - J_{\rm out}(T = T_m)$. This quantity determines the relative volume fractions of the melt and solid. There will be a 50-50 mixture of solid and liquid if $\Delta J = 0$. Increasing ΔJ will increase the fraction of the molten phase.

We introduce the dimensionless variables $t/\tau_0 \to t$, $r/\xi_0 \to r$, and $u\,L/(2\epsilon_0) \to u$. The dynamical equations become

$$\partial_t \phi = -\mu_B + \nabla^2 \phi + u, \qquad (2.6)$$

$$\partial_t u = D \nabla^2 u - \ell\, \partial_t \phi + \Delta j - r_0\, \phi, \qquad (2.7)$$

with the dimensionless parameters

$$D = \frac{\tau_0 K_T}{\xi_0^2 \rho_0 C_p}, \quad \ell = \frac{L^2}{4\epsilon_0 T_m C_p},$$

$$\Delta j = \frac{\tau_0 L \Delta J}{2\epsilon_0 h T_m \rho_0 C_p}, \quad r_0 = \frac{\tau_0 L J_0 \Delta R}{4\epsilon_0 h T_m \rho_0 C_p}. \qquad (2.8)$$

We will use these rescaled equations as our working model. There are four independent parameters. We discuss primarily the symmetric case, i.e., $\Delta j = 0$. Equations (2.6) and (2.7) with $r_0 = 0, \Delta j = 0$ have been used as models of phase ordering dynamics with conservation of order parameter [23].

III. ANALOGY WITH BLOCK COPOLYMERS

A. Dynamical equation and static states

The fundamental feature of laser induced melting is that there is local phase segregation but macroscopic phase separation is suppressed due to an effective long range interaction. This is a feature common of many physical systems. Therefore we ask whether there is a relationship between different models with this feature. In this section we show that in the limit of large latent heat the dynamics are equivalent to that of a model of block copolymers. In particular, the static configurations are always static configurations of the block copolymer model. Using this analogy we obtain the characteristic periodicity of the patterns using systematic expansions around two limits.

A block copolymer is a linear polymer chain consisting of two subchains A and B covalently bonded to each other. As the repulsion between A and B chains is increased there can be segregation of A and B chains. However, due to the covalent bonding macroscopic phase separation is impossible. Instead the static state consists of alternating A and B domains of mesoscopic size.

The free energy for block copolymers can be written in scaled form as [9,10]

$$F\{\phi\} = \int d\mathbf{r}\, \left[f(\phi(\mathbf{r})) + \frac{1}{2} |\boldsymbol{\nabla} \phi(\mathbf{r})|^2 \right] - \frac{B}{2} \int d\mathbf{r}\, d\mathbf{r}'\, \phi(\mathbf{r}') G(\mathbf{r}, \mathbf{r}') \phi(\mathbf{r}), \qquad (3.1)$$

where $B \sim 1/N^2$ with N being the degree of polymerization, ϕ is the difference in the local volume fraction of A and B monomers, $G(\mathbf{r}, \mathbf{r}')$ obeys $\nabla^2 G(\mathbf{r}, \mathbf{r}') = \delta(\mathbf{r} - \mathbf{r}')$, and f is a double well coarse-grained free energy. Other than symmetry considerations, the exact form of f is unimportant. We can choose it to be the same as that of our model for laser induced melting. Assuming relaxational dynamics, the dynamics for block copolymers is [12,22]

$$\frac{1}{\Gamma} \partial_t \phi = \nabla^2 \frac{\delta F}{\delta \phi} = \nabla^2 \left(\mu_B - \nabla^2 \phi \right) - B[\phi(\mathbf{r}) - \bar{\phi}], \qquad (3.2)$$

where $\mu_B = \partial f / \partial \phi$, $\bar{\phi}$ is the average value of ϕ, and Γ is a kinetic coefficient. The static solution obeys

$$0 = \nabla^2 \left(\mu_B - \nabla^2 \phi \right) - B[\phi(\mathbf{r}) - \bar{\phi}]. \qquad (3.3)$$

There are two regimes. For values of B very close to the onset of microphase separation, the size of the patterns grows as $B^{-1/4}$ [9,10]. This is called the weak segregation regime. Further from onset is the strong segregation regime in which the domain sizes grow as $B^{-1/3}$ [10,11,24(a)]. In this regime one typically observes a disordered lamellar structure unless the overall direction of the lamellae is fixed either by flow or by boundary conditions [22], or if the system is gradually annealed [24(b)].

Now we reconsider the laser induced melting model. We can use Eq. (2.6) to solve for u

$$u = \mu_B(\phi) - \nabla^2 \phi + \partial_t \phi. \qquad (3.4)$$

Substituting into Eq. (2.7) gives

$$\partial_t^2\phi + \ell\partial_t\phi + \frac{d\mu_B}{d\phi}\partial_t\phi - (D+1)\nabla^2\partial_t\phi$$

$$= D\nabla^2\left(\mu_B - \nabla^2\phi\right) + \Delta j - r_0\phi. \quad (3.5)$$

For $\ell \gg 1, \ell \gg D$, the left-hand side is dominated by the $\ell\partial_t\phi$ term and the dynamical equation becomes

$$\frac{\ell}{D}\partial_t\phi = \nabla^2\left(\mu_B - \nabla^2\phi\right) - \frac{r_0}{D}\left(\phi - \frac{\Delta j}{r_0}\right), \quad (3.6)$$

and is therefore equivalent to the *dynamics* of block copolymers [Eq. (3.2)] with $\Gamma = D/\ell$, $B = r_0/D$, and $\bar{\phi}B = \Delta j/D$. In addition, independent of the values of ℓ and D, the static solutions are extremums of the block copolymer free energy.

Figure 1 shows the ϕ configurations obtained from a simulation of the laser induced melting model. We will discuss the simulations in detail in later sections. Note that there are two regimes with qualitatively different patterns. In analogy with block copolymers we call these the strong and weak segregation regimes. On the left, the parameters corresponds to the weak segregation regime near onset. There are long parallel stripes straightening out in time. On the right, the parameters are further from onset. This corresponds to the strong segregation regime in block copolymers. Here a disordered lamellae structure is found. That is, rather than straight stripes, there is a more complicated interconnected structure. In this regime a cross section of the order-parameter profile would show domains of the two phases separated by a thin interfacial region over which the value of ϕ changes from $+1$ to -1.

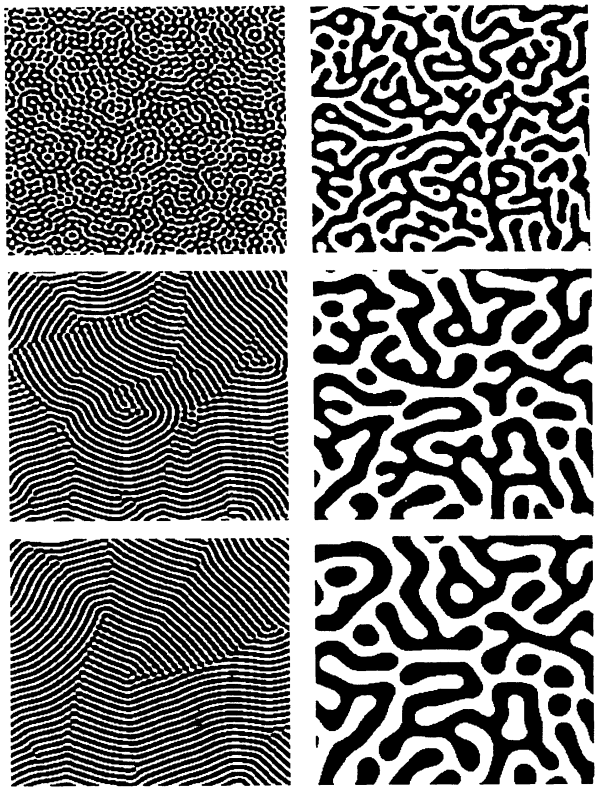

FIG. 1. The ϕ field for $L_x = L_y = 640$, $dx = 1.25$, $L = 2.0$, $D = 0.5$, and $\Delta j = 0$. A 256×256 portion of the 512×512 lattice is shown. From top to bottom, the left panels shows $r_0/D = 0.24$ (close to onset) with $t = 1600$, 12 800, and 10 2400. The rolls continue to straighten at later times. The right shows $r_0/D = 0.001\,875$ (far from the onset) for the same times. The patterns are essentially frozen after this time.

Using this analogy we will use known results for block copolymers to aid in our study of "laser induced melting." We will also use the laser induced melting model to shed some light on block copolymers. However, the dynamics for laser induced melting is richer. For example, if ℓ is not sufficiently large or D sufficiently small, the static solution is not obtained. Instead a time-dependent asymptotic state is reached which can be chaotic.

B. Energy minimization

The equilibrium length scale is the wavelength of the one-dimensional solution which minimizes the free energy. Let us assume a one-dimensional solution of wavenumber $k = 2\pi/\lambda$. We can write the free energy density as [11]

$$\frac{1}{\lambda}\int_{-\lambda/2}^{\lambda/2} dx \left[f(\phi) + \frac{1}{2}|\partial_x\phi|^2\right]$$

$$- \frac{B}{2\lambda}\int_{-\lambda/4}^{\lambda/4} dx \int_{-\lambda/4}^{\lambda/4} dx' \, |x - x'|\phi(x)\phi(x'), \quad (3.7)$$

where we choose $\phi(x) = -\phi(-x)$. In this subsection we demonstrate that the equilibrium length scales can be obtained via systematic expansions from the strong and weak segregation limits. We also show that in the strong segregation limit, this is equivalent to a modified form of the free energy arguments of Hawkins and Biegelsen [2].

1. *Strong segregation limit*

For small B the equilibrium length scale was obtained by Ohta and Kawasaki using a variational method by assuming a form for $\phi(x)$. We will show that this result can be justified via a systematic expansion in the small parameter $1/\lambda$. As shown in Appendix A, $\phi(x) = \pm 1 + \mathcal{O}(\lambda^{-1})$ in the two bulk phases. Near the interface $\phi(x) = \phi_0(x) + \mathcal{O}(\lambda^{-2})$ with ϕ_0 being the planar interfacial profile for $B = 0$. We can now calculate the free energy density. There are two interfaces per period so the local term in the free energy density is $2\bar{\sigma}/\lambda + \mathcal{O}(\lambda^{-2})$. The long range term is $B\lambda^2/96 + \mathcal{O}(\lambda^{-3})$. The free energy density is

$$\frac{F\{\phi\}}{\lambda} = \frac{2\bar{\sigma}}{\lambda} + \frac{\lambda^2 B}{96} + \mathcal{O}\left(\frac{1}{\lambda^2}\right). \quad (3.8)$$

[Here B is $\mathcal{O}(\lambda^{-3})$.] Minimizing F with respect to λ gives the wavelength of the one-dimensional solution with the lowest free energy as

$$\lambda^* = \left(\frac{96\bar{\sigma}}{B}\right)^{1/3} + \mathcal{O}(B^0). \tag{3.9}$$

This is in agreement with the previous strong segregation result for copolymers [10–12]. Higher order corrections can also be obtained to give

$$\lambda^* = \left(\frac{96\bar{\sigma}}{B}\right)^{1/3} + \frac{8\chi\bar{\sigma}}{5} + \mathcal{O}(B), \tag{3.10}$$

where $\chi^{-1} = d\mu_B/d\phi|_{\phi=1}$. The wavelength for the laser induced melting model is obtained by replacing B by r_0/D.

We can now see why the free energy describes the static states of laser induced melting by reconsidering an argument of Hawkins and Biegelsen [2]. In the strong segregation limit, the free energy density due to interfaces is $2\bar{\sigma}/\lambda$. They balanced this with the change in the entropic contribution TS (where S is the entropy) due to the superheating and undercooling of the bulk. In terms of the rescaled variables this contribution to the free energy density is $-\frac{1}{\lambda}\int_0^\lambda dx u(x)\phi(x) = \langle |u| \rangle$. Balancing these two factors they obtained $\lambda\langle |u| \rangle \approx 2\bar{\sigma}$. Note, however, that the static solution gives $u = (r_0/D)\nabla^{-2}\phi$, so that the long range term in block copolymer free energy is exactly this bulk entropic contribution. Therefore we have justified Hawkins and Beigelsen's approximate analysis. In fact, we can obtain the result [Eq. (3.9)] if we extend their argument by explicitly calculating $\langle |u| \rangle$ and minimizing the resulting free energy density.

For direct comparison with experiment the rescaling we have chosen is somewhat confusing in the small r_0 limit. In terms of the dimensional unscaled variables we find (leading order only)

$$\lambda^* = 4\left(\frac{6\sigma h T_m K_T}{\rho_0 L J_0 \Delta R}\right)^{1/3}, \tag{3.11}$$

so that the selected wavelength is independent of the microscopic parameters ξ_0, ϵ_0 and τ_0. As we will discuss in Sec. IV, this is $(6/27)^{1/3}$ of the result obtained by Jackson and Kurtze using a stability analysis of a periodic array of interfaces. Our result is in very close agreement with the experimental result of Dworschak and van Driel [6], although, due to the difference in the experimental geometry and the lack of symmetry between solid and liquid phases in the experiment, a very detailed comparison is not appropriate.

2. *Weak segregation limit*

We can also find the wavelength minimising the free energy in the weak segregation regime. The homogeneous state first becomes unstable at $B = B_0 = 1/4$ and wave number $k = k_0 = 1/\sqrt{2}$. Near onset, we can expand the static solution in orders of ϵ where $\epsilon^2 = B_0 - B$,

$$\phi(x) = \epsilon A_k \sin(kx) + \epsilon^3 A_{3k}\sin(3kx) + \mathcal{O}(\epsilon^5), \tag{3.12}$$

with $A_k^2 = (8/3)\{1 - 2[(k-k_0)/\epsilon]^2\}$ and $A_{3k} = 9A_k^3/128$. Here $k - k_0$ is assumed to be $\mathcal{O}(\epsilon)$. In this limit the free energy density is

$$\frac{F\{\phi\}}{\lambda} = -\frac{\epsilon^2 A_k^2}{4}\left(1-k^2\right) + \frac{\epsilon^4 3A_k^4}{32}\left(1-9k^2\right) + \frac{\epsilon^2 B A_k^2}{4k^2} + \mathcal{O}(\epsilon^6). \tag{3.13}$$

The first two terms correspond to the short range parts of the free energy density while the last term is the long range portion. We minimise this expression with respect to k to give

$$k^{*4} = B + \mathcal{O}(\epsilon^4), \tag{3.14}$$

which is in agreement with the previous weak segregation result [11,12,22]. The next order correction can also be calculated (one needs to keep terms of order ϵ^6 in the free energy) to give

$$k^{*4} = B\left(1 - \frac{5}{16}\epsilon^4\right) + \mathcal{O}(\epsilon^6). \tag{3.15}$$

We see that the fourth order correction is fairly small. In the weak segregation limit the selected wavelength depends on the microscopic parameters. In terms of the dimensional unscaled variables, the leading order result is

$$k^4 = \frac{L J_0 \Delta R}{4\epsilon_0 \xi_0^2 h T_m K_T}. \tag{3.16}$$

This limit cannot be obtained from the previous interface description.

IV. STABILITY ANALYSIS

A. Linear stability analysis

Since a Liapunov functional exists only in the large ℓ limit, in general, the laser induced melting model has much richer dynamics than the block copolymer model. Some insight into the dynamics can be obtained through a variety of stability analysis.

The homogeneous solution of Eqs. (2.6) and (2.7) is $\phi^* = \Delta j/r_0$, $u^* = \mu_B|_{\phi=\phi^*}$. We assume infinitesimal perturbations $\delta\phi_k = \delta_\phi \exp(\omega_k t + i\mathbf{k}\cdot\mathbf{r})$ and $\delta u_k = \delta_u \exp(\omega_k t + i\mathbf{k}\cdot\mathbf{r})$. Solving the dynamical equations (2.6) and (2.7) to first order in δ gives

$$\omega_k = -\frac{\gamma_k'}{2} + \frac{|\gamma_k'|}{2}\left(1 - \frac{4(r_0 + \gamma_k D k^2)}{\gamma_k'^2}\right)^{1/2}, \tag{4.1}$$

where $\gamma_k = \mu_B' + k^2$ with $\mu_B' = d\mu_B/d\phi|_{\phi=\phi^*}$ and $\gamma_k' = \ell + \gamma_k + Dk^2$.

For $\mu_B' > 0$, the real part of ω_k is always negative and the homogeneous state is linearly stable. In this case, the initial state is outside the spinodal. For $\mu_B' < 0$ the

linear dynamics can be divided into several classes. For $\ell < -\mu_B'$, the homogeneous system is linearly unstable to small wave number perturbations ($k \to 0$). If $4r_0 > (\ell + \mu_B')^2$ the instability will be oscillatory.

If $\ell > -\mu_B$ the system is linearly stable to small wave number perturbations. If, in addition, $r_0 > \max(-\gamma_k D k^2) = D(\mu_B'/2)^2$ the homogeneous state is linearly stable to perturbations of all wave numbers. For $r_0 < D(\mu_B'/2)^2$ the system will be unstable in a finite band of wave numbers,

$$-\mu_B' - \sqrt{(\mu_B')^2 - \frac{4r_0}{D}} < 2k^2 < -\mu_B' + \sqrt{(\mu_B')^2 - \frac{4r_0}{D}}. \tag{4.2}$$

For $\Delta j = 0$ and $\mu_B = -\phi + \phi^3$, the conditions are (i) unstable at $k = 0$ if $\ell < 1$, (ii) stable to all k if $r_0/D > 1/4$, and (iii) if $r_0/D < 1/4$ then unstable in a band of wave number k with $1/2 - \sqrt{1/4 - r_0/D} < k^2 < 1/2 + \sqrt{1/4 - r_0/D}$.

B. Phase diffusion description

1. Stability of lamellae

The state minimizing the block copolymer free energy corresponds to parallel stripes. The approach to this state is via locally parallel lamellae with the orientation and wave number varying slowly on the length scale of the patterns (although we do not assume a global orientation). The dynamics of the lamellae are described by the phase-diffusion formalism [25(a),20]. This formalism allows the classification of the stability of the lamellae as well as a rigourous criteria for wave number selection. In this section we obtain the phase diffusion equations for the laser induced melting model and discuss the stability of the slowly varying lamellae state. Using this description we obtain the characteristic length scale in agreement with the block copolymer length scale and discuss a new instability which we conjecture to be a signal of time-dependent chaotic dynamics.

Since we are interested in behavior on length scales much larger than the wavelength of the stripes, we need to separate the long distance, large time behavior on this length scale from the short length-scale behavior. To see how this is done, note that at each point in the stripe pattern we can define the local wave vector $\mathbf{k}(\mathbf{r}, t)$ which is directed in the direction normal to the stripes and whose magnitude is the local wave number of the stripes. Locally the choice of this vector is twofold degenerate (i.e., we can choose either $\mathbf{k}$ or $-\mathbf{k}$). However, once this choice is made at one point it is fixed at all points. We assume that $\mathbf{k}$ varies on length scales $1/\tilde{\epsilon}$, much larger than the pattern wavelength $2\pi/k$. (Here we use $\tilde{\epsilon}$ as the small parameter to avoid any confusion with the previous ϵ.) We can now introduce the slow space and time variables via

$$\mathbf{X} = \tilde{\epsilon}\mathbf{r}, \quad T = \tilde{\epsilon}^2 t \tag{4.3}$$

and the fast phase variable $\theta(\mathbf{r}, t)$, such that $\theta = n\pi$ at each solid-liquid interface. We can relate the local wavevector $\mathbf{k}$ to the fast variable θ by

$$\mathbf{k}(\mathbf{X}, T) = \nabla\theta(\mathbf{r}, t). \tag{4.4}$$

The goal of the phase diffusion description is to describe the slow dynamics of $\mathbf{k}$ on the long length scales $\mathbf{X}$. The introduction of the separate slow and fast variables allows us to write the dynamics order by order in $\tilde{\epsilon}$. The equilibrium free energy in terms of the phase variables has been discussed by Kawasaki and Ohta [25(b)].

In terms of the phase variable the dynamical fields are of the form

$$\phi(\mathbf{r}, t) = \phi_k[\theta(\mathbf{r}, t)], \quad u(\mathbf{r}, t) = u_k[\theta(\mathbf{r}, t)], \tag{4.5}$$

where ϕ_k and u_k are 2π-periodic functions which are one-dimensional time-independent solutions with wave number k. Since static solutions exists for a band of wave numbers, ϕ_k and u_k depend on the local wave number and hence the slow variables $\mathbf{X}$ and T. The full derivation is given in Appendix B. Here we only give the final results. The dynamics for the phase variable θ is

$$\tau_k\, \partial_t\theta = -\nabla \cdot \mathbf{k}\, G(k), \tag{4.6}$$

where

$$G(k) = \frac{D}{r_0} A_u(k) q_{u,k} - A_\phi(k) q_{\phi,k} \tag{4.7}$$

and

$$\begin{aligned}\tau_k &= A_\phi(k)\left(q_{\phi,k} + \frac{\ell}{Dk^2}\right) - \frac{1}{r_0} A_u(k) q_{u,k} \\ &= \frac{D-1}{r_0} A_u(k) q_{u,k} + \frac{\ell}{Dk^2} A_\phi(k) - G(k).\end{aligned} \tag{4.8}$$

The coefficients are related to the static one-dimensional solutions by

$$\begin{aligned} A_\phi(k) &= \frac{1}{2\pi}\int_0^{2\pi} d\theta\, \phi_k(\theta)^2, \\ A_\phi(k) q_{\phi,k} &= \frac{1}{2\pi}\int_0^{2\pi} d\theta\, [\partial_\theta \phi_k(\theta)]^2, \\ A_u(k) &= \frac{1}{2\pi}\int_0^{2\pi} d\theta\, u_k(\theta)^2, \\ A_u(k) q_{u,k} &= \frac{1}{2\pi}\int_0^{2\pi} d\theta\, [\partial_\theta u_k(\theta)]^2. \end{aligned} \tag{4.9}$$

Since ϕ_k and u_k depend on $k(\mathbf{X}, T)$ these coefficients depend on the slow variables.

The stability condition is apparent in curvilinear coordinates [20]. Let w be the distance in the normal direction and $\mathbf{s}$ be that in the tangential directions. In curvilinear coordinates the first order phase diffusion dynamics [Eq. (4.6)] becomes

$$\tau_k \partial_t\theta = D_w \partial_w^2\theta + D_s \nabla_s^2\theta, \tag{4.10}$$

where $D_w = -d[kG(k)]/dk$ and $D_s = -G(k)$. The sys-

tem is stable against slow variations of the local wave number (the Eckhaus instability) if $\tau_k^{-1}D_w > 0$, while the lamellae is stable against variations in the orientation (the zigzag instability) if $\tau_k^{-1}D_s > 0$. If $\tau_k > 0$ and one neglects defects, the functional [20]

$$F\{k(\mathbf{r},t)\} = \int d\mathbf{r} \int_0^{k(\mathbf{r},t)^2} dq^2 G(q) \tag{4.11}$$

defines a Liapunov functional with the extremum $G(k^*) = -D_{\|} = 0$. Therefore the selected length scale is exactly the one marginally stable against the zigzag instability. Since, for ordered lamellae, this wavelength is unique, it must be the same as the block copolymer length scale.

For some parameters, τ_k can be negative. If this occurs at larger wave number than that at which D_s and D_w becomes negative, the lamellae will become unstable to both the zigzag and Eckhaus instabilities simultaneously. That is both, $\tau_k^{-1}D_s(k)$ and $\tau_k^{-1}D_w(k)$ become negative at the same k. From Eq. (4.8) this simultaneous instability supersedes the isolated zigzag instability if the latent heat is sufficiently small,

$$\ell < (1-D)\frac{Dk^{*2}A_u(k^*)q_{u,k^*}}{r_0 A_\phi(k^*)}, \tag{4.12}$$

where k^* is the wave number at which the zigzag instability occurs, i.e., $D_s(k^*) = 0$. Small ℓ is exactly the condition for which the analogy with the relaxational block copolymer dynamics does not hold. From the phase diffusion dynamics, we cannot determine the final evolution of the unstable state. However, the lamellae are unstable to perturbations of wave number q in an entire band of wave numbers around $q = 0$. So we conjecture that this may be a signal of time-dependent dynamics. Note that this is not the skewed-varicose instability [26] which has also been suggested as a signal of a time-dependent asymptotic state [27,28]. The skewed-varicose instability is also a long wavelength instability to perturbations with components both normal and tangential to the stripes. However, the skewed-varicose instability occurs at a fixed angle, i.e., fixed ratio of the normal and tangential components of the perturbation. In this case, the lamellae is unstable to perturbations with an arbitrary ratio of normal and tangential components.

In general, the coefficients $A_\phi(k)$, $A_u(k)$ and $q_{\phi,k}$, $q_{u,k}$ must be obtained numerically. However, they can be obtained explicitly in the strong and weak segregation limits. In particular, since these coefficients depend only on the static one-dimensional solutions we can use the results of Appendix A. (It turns out to be calculationally simpler to obtain the selected wavelength using this criterion rather than minimizing the free energy.)

2. *Strong segregation limit*

In the thin interface limit, we can use the static solution in Appendix A to calculate the coefficients $A_\phi(k)$, $q_{\phi,k}$, $A_u(k)$, and $q_{u,k}$ order by order in $\mathcal{O}(\lambda^{-1}) = \mathcal{O}((r_0/D)^{1/3})$. Details are given in Appendix B. We find that

$$G(k) = -D_s = \frac{r_0}{D}\frac{\pi^2}{12k^4} - \frac{1}{60}\left(\frac{r_0}{D}\right)^2 \frac{\chi\pi^4}{k^6} - \frac{\sigma}{\pi k} + \mathcal{O}(\lambda^{-1}), \tag{4.13}$$

where $\chi^{-1} = d\mu_B/d\phi|_{\phi=1}$. Here we have kept the leading- and next-leading-order terms. The diffusion constant in the normal direction is

$$\frac{d}{dk}kG(k) = -D_w = -\frac{\pi^2 r_0}{4Dk^4} + \frac{1}{6}\left(\frac{r_0}{D}\right)^2 \frac{\chi\pi^4}{k^6} + \mathcal{O}(\lambda^{-1}). \tag{4.14}$$

The leading order $D_w > 0$, and the system is stable to the Eckhaus instability at that order. The kinetic coefficient τ_k is

$$\tau_k = \left(\frac{D-1}{D}\right)\frac{\sigma}{\pi k} + \frac{\ell}{Dk^2} - G(k) + \mathcal{O}(\lambda^{-1}). \tag{4.15}$$

The lamellar is unstable to the zigzag instability [$G(k) < 0$] for $\lambda > \lambda^*$ where

$$\lambda^* = \frac{2\pi}{k^*} = \left(\frac{96D\bar{\sigma}}{r_0}\right)^{1/3} + \frac{8\chi\bar{\sigma}}{5} + \mathcal{O}(\lambda^{-1}). \tag{4.16}$$

This length scale is in agreement with the result in Sec. III. Since $dkG(k)/dk < 0$ for all regions where $G(k) < 0$, the lamellae is effectively stable against a separate Eckhaus instabilities.

We now relate our result to the interfacial stability analysis of Jackson and Kurtze [8]. They considered the stability of a periodic array of stripes using a phenomenological interfacial description, i.e., the kinetics of the temperature field was given by Eq. (2.3) and its value at the interface was fixed by the local equilibrium Gibbs-Thomson condition. The interfacial velocity was related to the energy current by conservation of energy. They discussed the dynamics of an infinitesimal perturbation of wave number q in the orientation of the stripes. Due to the undercooling (superheating) the stripes can be unstable to the Mullins-Sekerka instability [29]. However, for low q, they found that the interface is stable because the energy flux is decreased (increased) if the liquid phase advances (recedes) into the solid phase. At large q the interface is stable due to surface tension. The two stable bands overlap only if the wavelength of the stripes lies within a specific range. Therefore the selected wavelength must be within this stable band. The largest wavelength in the stable band was a factor of $(27/6)^{1/3}$ larger than that given by Eq. (4.16).

In our analysis we also find a stable range of wave numbers, but we explicitly showed that the selected wavelength is exactly the largest wavelength in the band, i.e., the wavelength marginally unstable to the zigzag instability. Moreover, we do not find the stability to perturbations of low q. The reason for this difference is that Jackson and Kurtze discussed the stability of a single

stripe independent of the rest of the system. Here we have considered collective behavior of an entire set of stripes. Their analysis can be obtained from ours if we consider a perturbation with a component in the normal direction $q_w = \mathcal{O}(1/\lambda)$. Since the normal diffusion constant D_w is positive, this means the interface is stable to perturbations of this type at small tangential wave number q_s. Furthermore due to this stabilizing effect, the stripe wavelength at which the instability occurs is larger than that of the zigzag instability. In fact, Jackson and Kurtze commented that preliminary estimates including cooperative behavior gives a largest stable wavelength approximately 2/3 that of the independent stripe analysis [8].

The lamellae can become unstable to both the Eckhaus and zigzag instability simultaneously if τ_k becomes negative while both D_s and D_w are positive. We find this instability supersedes (i.e., occurs at higher wave number) the independent zigzag instability if

$$\ell < (1-D)\frac{\bar{\sigma}}{\pi}k^* = (1-D)\left(\frac{\bar{\sigma}^2 r_0}{12D}\right)^{1/3}. \qquad (4.17)$$

3. *Weak segregation limit*

We can also obtain the phase equations in the weak segregation limit. As shown in Appendix A, the static solution can be obtained order by order in ϵ where $\epsilon^2 = 1/4 - B$. The coefficients are given in Appendix B. The result is

$$G(k) = \frac{\epsilon^2 A_k^2}{2}\left[1 - \frac{r_0}{Dk^4} + \epsilon^4\left(\frac{3A_k^2}{128}\right)^2\left(81 - \frac{r_0}{Dk^4}\right)\right] + \mathcal{O}(\epsilon^8), \qquad (4.18)$$

where $A_k^2 = (8/3)\{1 - 2[(k-k_0)/\epsilon]^2\}$. The lamellae becomes unstable to the zigzag instability at

$$k^{*4} = B - \frac{5}{64}\epsilon^4 + \mathcal{O}(\epsilon^6), \qquad (4.19)$$

which is in agreement with the result for the equilibrium wavelength. $G(k)$ can also vanish if $A(k) = 0$. This gives an upper k limit to the stability band which occurs at

$$k^* = k_0 + \frac{\epsilon}{\sqrt{2}} + \mathcal{O}(\epsilon^2). \qquad (4.20)$$

Here we have only kept the leading order. To this order this k^* is equivalent to the neutral stability curve. This wave number corresponds to a local maxima in the Liapunov functional.

To find the simultaneous Eckhaus-zigzag instability we calculate τ_k to leading order

$$\tau_k = \epsilon^2 A_k^2 \frac{r_0}{D}\frac{D-1}{2Dk^4} + \epsilon^2 A_k^2 \frac{\ell}{2Dk^2} - G(k) + \mathcal{O}(\epsilon^6). \qquad (4.21)$$

Therefore in the weak segregation limit the system becomes unstable to both Eckhaus and zigzag instabilities simultaneously if $\ell < (1-D)\,(r_0/D)^{1/2}$.

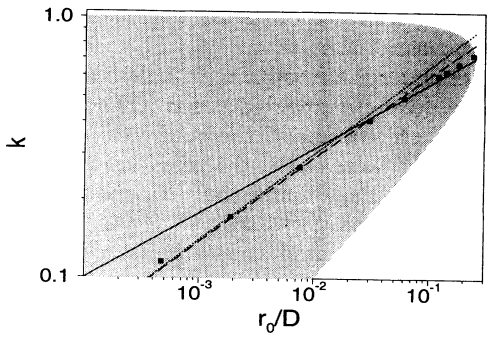

FIG. 2. Graphical summary of the stability analysis. The homogeneous state is linearly unstable within the shaded area. The solid line is $k^* = (r_0/D)^{1/4}$, i.e., the lowest order result for the selected wave number obtained near onset. The dotted line is the lowest order wave number far from onset $k^* = 2\pi(96D\bar{\sigma}/r_0)^{-1/3}$. The dashed line is the far from onset result including next order corrections. The squares are the length scale obtained from simulations with $\ell = 2$ and $D = 0.5$.

We summarize the results of the stability analysis in Fig. 2 in the large ℓ limit. We show the neutral stability curve $|k - k_0| = \sqrt{r_0/D}$ as well as the boundaries of the zigzag instability (and therefore the selected length-scale) as determined by the expansions around the weak and strong segregation limits.

V. NUMERICAL RESULTS

A. Previous numerical works

In this section we discuss the evolution of our model from an initial random small amplitude state. Previous related studies included numerical quenches of Raleigh-Bénard convection [30,31,19] and block copolymers [12,22].

Manneville [30] integrated the Swift-Hohenberg equation [32] and other two-dimensional models of Raleigh-Bénard convection starting from a small amplitude initial state. To mimic experiments the study was performed in a circular geometry. He characterized the linear and weakly nonlinear regimes and studied qualitatively the behavior of defects. Greenside and Coughran [31] were able to study a larger system and therefore make a more extensive analysis. They found that, near onset, the defects evolved to the boundaries leaving a defect-free region in the middle. However, further from onset, defects in the system tended to freeze and the boundaries become less important. The description of parallel roll regions separated by defects become less definite. The qualitative difference in the defect behavior was also shown by studying specially prepared initial conditions. For a pair of disinclinations, they found that, near onset, the disinclinations annihilate while far from onset, the disinclinations persists forever [31].

More recently, Elder *et al.* studied the evolution of

rolls following a quench of the Swift-Hohenberg equation with a stochastic noise term [19]. They found that the system can undergo a Kosterlitz-Thouless-type transition as the noise strength is varied. That is, for low noise amplitude, the orientation of the rolls exhibit long range order, while for large noise, the orientational correlation length is finite. They found that the width of the scattering intensity peak decreases as $t^{-1/4}$ in time implying that regions of correlated stripes grow as $t^{1/4}$. Using a projection method to describe the roll motion they found a small but nonvanishing coefficient for D_s indicating a transition to $t^{1/2}$ growth at very late times, though giving an effective $t^{1/4}$ growth at intermediate times [19]. However, the phase diffusion equations are the same generic form for the Swift-Hohenberg equations [20,21] as for our model. The selected wave number will therefore be that marginally stable against the zigzag instability, i.e., the k at which D_s vanishes. Based on the phase diffusion description we do not expect a crossover to $t^{1/2}$ growth at late times.

Oono and Bahiana considered the behavior of the dynamical model of block copolymers [Eq. (3.2)] following a quench from an initially disordered state [12,22]. They found a disordered lamellae pattern and show that neither including a bending modulus nor thermal fluctuations was sufficient to straighten out the patterns, although straightening can occur due to boundary conditions and due to the presence of flow [22]. Numerically they were only able to study not too small B and found $\lambda \sim B^{-1/4}$. However, using an analogy with phase ordering they argued that $\lambda \sim B^{-1/3}$ for small B. Liu and Goldenfeld also constructed a scaling function [11] to describe the behavior of the characteristic length scale as a function of B and time t after the quench. This scaling hypothesis was partially confirmed [22].

B. Selected length scale

We numerically updated the coupled partial differential equations (2.6) and (2.7) using an Euler discretization with mesh size $dx = 1.25$, time step $dt = 0.2$, and a sphericalized Laplacian (see Appendix C for details). We used 512×512 lattices with smaller lattices to test for finite size effects. Our simulations were restricted to the symmetric case ($\Delta j = 0$) and fixed $D = 0.5$. For the initial set of simulations we fixed $\ell = 2$. This value of ℓ was sufficiently large so that the copolymer analogy is applicable and a static state is always reached. Most of the runs were to $t = 102\,400$ or about 500 000 updates. For selected cases, we ran to $t = 256\,000$. We chose an uncorrelated Gaussian distribution for the initial values of ϕ with mean zero and deviation of 0.001. The u field was set to zero initially. If we start with an average u different from zero, the system rapidly evolved so that the average was zero. Even starting with a different value of average ϕ did not have a major effect unless the value was outside the spinodal. Unfortunately, due to the length and size of the simulation we were only able to average over two to four initial conditions depending on the parameters.

In Fig. 1 we showed that there are two regimes displaying qualitatively different behavior. Near onset, the system evolves to locally parallel rolls with the wave number fixed near that maximizing the linear instability, i.e., $k_0 = 1/\sqrt{2}$. The parallel rolls then slowly straighten out in time. As shown in Fig. 3(a), ϕ and u are relatively small amplitude and approximately sinusoidal justifying our near onset analysis. As expected u is negative (positive) where ϕ is positive (negative) so that the solid phase ($\phi < 0$) is superheated and the liquid phase ($\phi > 0$) is undercooled. Far from onset [Fig. 3(b)] the characteristic wave number slowly decreases with time and is much less than k_0. There does not seem to be any tendency toward locally parallel rolls and the system freezes into a disordered lamellar structure. The solid phase is superheated and liquid phase undercooled. The ϕ field can be divided into bulk and interfacial areas where ϕ changes rapidly from one bulk value to another while u is smooth.

Figure 4 shows the circular average scattering intensity $S_k = \langle \phi_k \phi_{-k} \rangle$ for the order-parameter field for the same values of r_0/D. Near onset, the wave number of the very sharp peak is fixed in time. Far from onset, we observe a much broader peak which moves, with time, toward lower wave number. This is indicative of the growing characteristic wavelength of the patterns and the disordered structure observed far from onset. Similar scattering intensities have been observed experimentally by Dworschak and van Driel [6].

As a quantitative measure of the characteristic wavenumber we chose a quantity that amplifies the contribution from the peak in S_k. For each value of r_0/D we calculated

$$k_1 = \frac{\int_0^\infty dk\, k\, S_k^2}{\int_0^\infty dk\, S_k^2}. \tag{5.1}$$

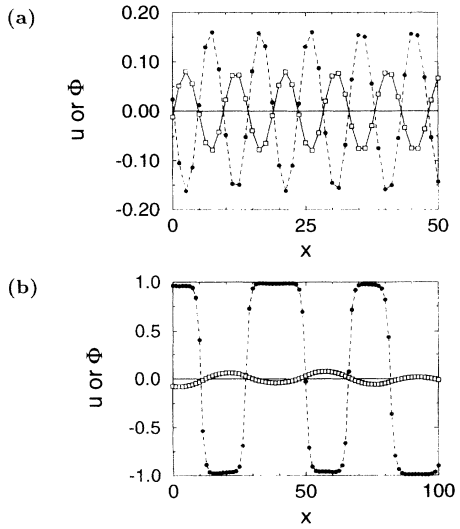

FIG. 3. The values of the ϕ and u field along a horizontal cut for two values of r_0/D. The dashed line with the solid circles is the ϕ field while the solid line with open boxes is the u field. (a) $r_0/D = 0.24$ (near onset). (b) $r_0/D = 0.001\,875$ (far from onset).

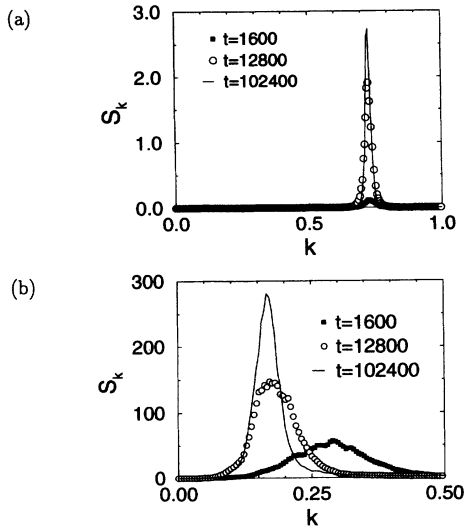

FIG. 4. The circular averaged scattering intensities $S_k(t)$ for $t = 1600$, 12 800, and 102 400. (a) $r_0/D = 0.24$ (close to onset). The sharp peak in $S_k(t)$ is fixed at $k \approx 0.7$. (b) $r_0/D = 0.001\,875$. The broad peak shifts toward lower k with time.

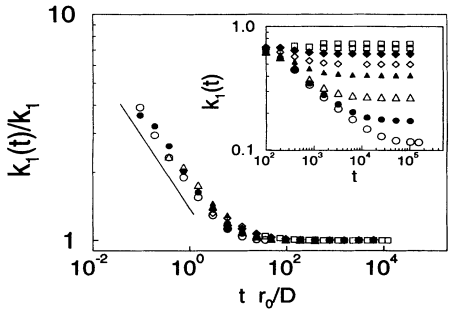

FIG. 5. Test of the scaling form $k_1(t) = k_1(\infty)g(tr_0/D)$. Plot is of $k_1(t)/k_1(\infty)$ vs r_0/D for seven values of r_0/D from 0.000 468 75 to 0.24. The line is of the form $k \sim t^{1/3}$. The inset shows the unscaled plot of $k_1(t)$ vs t.

The squares in Fig. 2 show k_1 vs r_0/D for various values of r_0. Also shown are the selected wavelengths obtained from the stability analysis; the selected wavelengths obtained from the free energy minimization are the same. We show the lowest order and next order result from the far from onset expansion, but only the lowest order result for the near onset expansion since the next order correction is negligible where this is valid. There is very good agreement between the theoretical prediction and k_1 in the simulation. In particular, we observe both limits of the strong segregation regime in which $k \sim (r_0/D)^{1/3}$ and the weak segregation regime for which $k \sim (r_0/D)^{1/4}$.

Liu and Goldenfeld have conjectured that the characteristic wavenumber has the following scaling form [11]:

$$k(t, B) = k_\infty(B)g(tB), \tag{5.2}$$

where, using the block copolymer notation, $B = r_0/D$ and $g(x)$ is a dimensionless scaling function that behaves as $x^{-1/3}$ for small x. This conjecture was based on dimensional analysis of the block copolymer equations and the analogy with phase ordering dynamics. They numerically tested this by plotting $k(t, B)/k_\infty$ vs tB and found a good collapse [11,22]. However, for small B they were not able to obtain the asymptotic wave number k_∞ directly and they chose $k_1(\infty)$ to produce the best collapse. Therefore it is not entirely clear that Eq. (5.2) is obeyed. In fact, it is simple to see that this scaling form cannot hold for all B and t. For B near onset $k(t)$ is approximately $k_0 = \sqrt{2}$ from the very earliest to latest times. Therefore near onset, $g(x)$ is a constant for all x. Furthermore the time scales over which linear dynamics hold t_{lin} can be made arbitrary large by decreasing the amplitude of the initial condition. There must be an offset in time which depends on t_{lin}.

Therefore this scaling form can hold only if we impose the constraint that $t \gg t_{\text{lin}}$ and $k_1 < k_0$. In Fig. 5 we plot $k_1(t)/k_1(\infty)$ vs tr_0/D for values of r_0/D ranging from 0.000 468 75 and 0.24 where $k_1(\infty)$ are the values shown in Fig. 2. We find a reasonable collapse of data over this regime although, due to the small number of configurations, the scatter is quite large. In the strong segregation limit, one expects that the small value of r_0/D is irrelevant at early times and we recover the result for spinodal decomposition with conservation of order parameter, i.e., $k_1(t) \sim t^{-1/3}$ or $g(x) \sim x^{1/3}$ [11]. Therefore, with the restrictions discussed, which essentially means that the scaling relation is only nontrivial not too close to onset, our data are consistent with the scaling form of Liu and Goldenfeld [11].

C. Orientation correlations

To further quantify the difference in the strong and weak segregation regimes we construct the director field for the stripes. The stripes pattern can be describe by a liquid crystal type order parameter [18]. To construct the director field, we cannot use the local gradient since it will vanish at maximum and minimum of the stripe pattern. Instead we use a symmetric difference to determine the direction tangential to the stripes. We define at each lattice point i, j the differences

$$\begin{aligned}
\Delta(0) &= |u_{i,j} - u_{i+1,j}| + |u_{i,j} - u_{i-1,j}|, \\
\Delta(\pi/4) &= \frac{1}{\sqrt{2}}\Big(|u_{i,j} - u_{i+1,j+1}| + |u_{i,j} - u_{i-1,j-1}|\Big), \\
\Delta(\pi/2) &= |u_{i,j} - u_{i,j+1}| + |u_{i,j} - u_{i,j-1}|, \\
\Delta(3\pi/4) &= \frac{1}{\sqrt{2}}\Big(|u_{i,j} - u_{i+1,j-1}| + |u_{i,j} - u_{i-1,j+1}|\Big).
\end{aligned} \tag{5.3}$$

We then define θ as the angle minimizing $\Delta(\theta)$. This is obtained by finding the m^* minimizing $\Delta(m\pi/4)$ and making a quadratic fit to $\Delta[(m^*+1)\pi/4]$, $\Delta(m*\pi/4)$, and $\Delta[(m^*-1)\pi/4]$. Hence θ is in the direction in which the change in $|u|$ is the smallest (tangential to the stripes).

We use u, since for r_0/D, ϕ is effectively discontinuous on length scales larger than the interfacial width.

The orientational correlation function measures the changes in orientation of the stripes. We define it as

$$C_\theta(\mathbf{r}) = \langle \exp[i2\theta(\mathbf{R}+\mathbf{r})] \exp[i2\theta(\mathbf{r})] \rangle, \quad (5.4)$$

where the angular brackets indicate an average over initial conditions or, for sufficiently large systems, a translational average over $\mathbf{R}$. The factor of 2 is required since the director is a headless vector and has a twofold symmetry.

As might be expected the qualitative difference between the behavior close to onset and far from onset is magnified in the director field. Figure 6 shows the director field for $r_0/D = 0.24$ for the same times as in Fig. 1. At $t = 1600$, the system is barely out of the linear dynamics stage and one observes essentially randomly oriented regions. Patches of correlated regions form and grow with time. By $t = 12\,800$ the correlated regions are already on the order of the system size. The patches continue to grow but one observes long lived structures indicating the presence of grain boundaries and defects.

Figure 7(a) shows $C_\theta(x)$ near onset, $r_0/D = 0.24$, and $t = 800$, 1600, 3200, 4800, 6400, and 12 800. C_θ coincide for the first two times since they are just beyond the linear regime. For $t \geq 12\,800$ the orientational correlation length is very large and strong finite size effects are found. As shown in the inset, there are two characteristic length scales evident in C_θ. There is a kink in C_θ at approximately $x \sim 3$ and then a slow decay at larger x. We interpret this kink as the contribution arising from the defect cores while the slow decay comes from the slow variations in the orientation. With increasing time the contribution from the "defects" decreases, reflecting the decrease in the density of defects. This is consistent with our qualitative analysis of the patterns.

Figure 7(b) shows $C_\theta(r)$ far from onset, r_0/D =

FIG. 6. The director field for $r_0/D = 0.24$ corresponding to the same times as in Fig. 1 ($t = 1600, 12\,800$, and $102\,400$.). The entire 512×512 lattice is shown. The lower left quarter box corresponds to the 256×256 region shown in Fig. 1. White denotes regions with $\cos(2\theta) > 0$ ($-\pi/2 < 2\theta < \pi/2$) and black denotes $\cos(2\theta) < 0$.

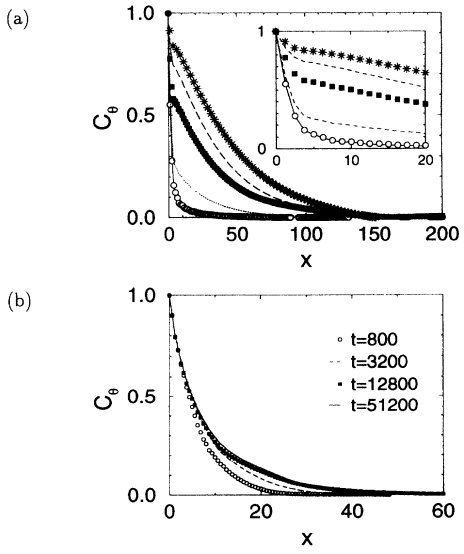

FIG. 7. The orientational correlation function C_θ. (a) C_θ near onset ($r_0/D = 0.24$) with times $t = 800$ (−), 1600 (○), 3200 (···), 4800 (•), 6400 (—), and 12 800 (∗). The inset is the region near $x = 0$. (b) C_θ further from onset ($r_0/D = 0.001\,875$). Times $t = 800$, 3200, 12 800, and 51 200 are shown.

0.001 875. Times $t = 800, 3200, 12\,800$, and $102\,400$ are shown. In contrast to the near onset case, there is no kink at short length scales since pattern can no longer be described by regions of locally parallel lamellae separated by defects. The orientational correlational length is much smaller than for that near onset and grows slowly in time. This growth is due mainly to the growth of the characteristic pattern size during this time.

To quantify the behavior further, we define the orientational correlation length $L_\theta(t)$ as the value of x at which $C_\theta(x)$ reaches the value of $1/e$ [note that $C_\theta(0) = 1$]. Figure 8 shows $L_\theta(t)$ for $r_0/D = 0.06, 0.12, 0.18$, and 0.24. Very close to onset ($r_0/D = 0.18$ and 0.24), L_θ is consistent with the power law growth $L_\theta \sim t^{1/4}$ as observed by Elder *et al.* [19] in a quench of the Swift-Hohenberg equation. However, with decreasing r_0/D we find that L_θ saturates at a value which depends on r_0/D and is much smaller than the system size, although asymptotic logarithmic growth cannot be ruled out.

Figure 9 is a plot of asymptotic value of the product $L_\theta k_1$ as a function of r_0/D. For the two values of r_0/D near onset L_θ continues to grow so that the points are not the saturation values. Several features are evident. The product $L_\theta k_1$ approaches a well define limit of order unity as r_0/D approaches zero. This is the thin interface regime in which there is single length scaling with the orientational correlation length being on the same order as the characteristic wavelength of the patterns. Closer to onset, the system cannot be described by a single length scale, but instead both the characteristic pattern size and the orientational correlational length are required. The orientational correlation length becomes much larger than the pattern size as $r_0/D \to 1/4$.

Several interpretations are possible. First, $L_\theta(t)$ may grow as a power law $L_\theta(t) \sim t^{1/4}$ up to some finite saturation value depending on r_0/D. Candidates for this saturation length are the length scales on which defects and boundary effects heal [33]. Near onset, the perturbation due to a defect will disappear on length scales of ϵ^{-1} in the direction normal to the stripes and $\epsilon^{-1/2}$ in the direction tangential to the stripes ($\epsilon^2 = 1/4 - r_0/D$). The distinction in the two directions is due to the vanishing of the tangential diffusion constant at the selected wavenumber. Estimates of the first length scale gives

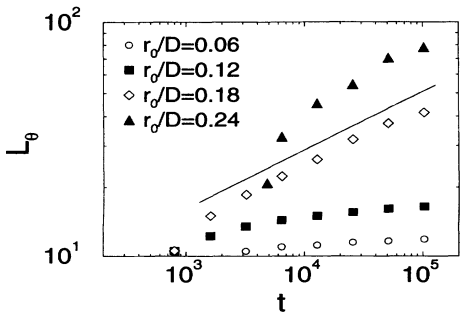

FIG. 8. The orientational correlation length $L_\theta(t)$ for $r_0/D = 0.06$, 0.12, 0.18, and 0.24 on a log-log scale. A line of $L \sim t^{1/4}$ is also drawn. The data for $r_0/D = 0.24$ are strongly influenced by finite size effects.

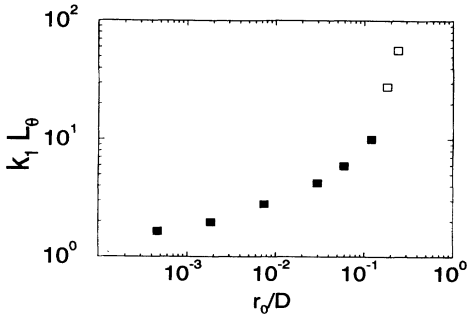

FIG. 9. The orientational correlation length $L_\theta k_1$ for eight values of r_0/D ranging from $r_0/D = 0.000\,468\,75$ to $r_0/D = 0.24$ on a log-log scale. This product is expected to be approaching its asymptotic values except for two points closest to onset (open squares).

~ 10 for $r_0/D = 0.24$ and 3.7 for $r_0/D = 0.18$. Estimates of the tangential length scale gives ~ 3 and ~ 2, respectively. Although these candidates cannot be ruled out, they are much smaller than that for the observed orientational correlation length. These lengths are equivalent to the equilibrium or steady state correlation length on which the effect of fluctuations decay [18].

A second possibility is that the orientational correlation length grows as a power law in time for small t and then crosses over to logarithmic growth at larger time with the crossover length depending on r_0/D. This slow growth will then continue until limited by the system size. It would indicate that the long time scale dynamics are similar to that of a magnetic system in a random field, perhaps because the long-lived defects are effectively quenched-in impurities. Based on our simulations we cannot rule this out. This crossover length scale may be related to steady state correlation length described above.

The third possibility is the most intriguing. According to simulations of the Swift-Hohenberg equation by Elder *et al.* [19], the system shows long range orientational correlational ordering at a finite distance from onset. That is, the orientational correlation length is limited only by the system size. On the other hand, our results indicate that, further from onset, the orientational correlation length is finite and much smaller than the system size. If this is the case then there will be a value of $r_0/D < 1/4$ at which the orientational correlation length becomes finite (in an infinite system). This would mark the presence of a nonequilibrium phase transition similar to a glass transition. Note that this transition cannot be an equilibrium phase transition since the lowest free energy state is that of parallel stripes. In addition, this transition, if it exists, must depend on dynamical features such as quench rate, the presence of walls, and in a real system, impurities. Although such a possibility is intriguing, based on our numerical results, we cannot differentiate between this scenario and other scenarios based on an effective crossover length approaching infinity as $r_0/D \to 1/4$ in which case there is no secondary transition for $r_0/D < 1/4$. To tell which of these scenar-

ios, if any, occur one must simulate larger systems with more initial configurations and with a systematic finite size analysis.

D. Time-dependent asymptotic states

In the limit of large latent heat the laser induced melting model is equivalent to a dynamical model of block copolymers which has a Liapunov functional and, therefore, purely relaxational dynamics. In this limit, there can be no motion of the patterns in the asymptotic state. However, as the latent heat is decreased the dynamics of the laser induced melting becomes distinctly different.

For illustrative purposes we discuss what happens as ℓ is decreased for particular values of $r_0 = 0.03$ and $D = 0.5$. There is very little change in the pattern dynamics as ℓ is decreased from 2 to 1. We monitor $\bar{\phi}(t) = \sum_{i,j} \phi_{i,j}(t)/(n_x n_y)$, i.e., the average value of ϕ, as a function of time. As ℓ is decreased below unity there are small oscillations of $\bar{\phi}$ at early times. These oscillations decay after one or two cycles and a disordered lamellar pattern is formed similar to that for $\ell = 2$. As ℓ is decreased further, below 0.6, there is a large increase in the amplitude of the oscillations as well as in the time for which oscillations persist. The corresponding patterns during this transient period consists of regions of disordered stripes intermingled with oscillating structures. For $\ell < 0.5$, there is a long transient period with a chaotic space time pattern. This transient dynamics persists for many periods but the system eventually evolves to a state that is homogeneous in space but oscillating in time.

For $r_0 = 0.03$ and $L_x = L_y = 160$, we can locate the transition to within $\Delta\ell = 0.05$. We always find the stripe phase for $\ell = 0.55$ and the oscillating homogeneous phase for $\ell = 0.5$. Depending on initial conditions, states for ℓ between these two values may settle into a inhomogeneous state consisting of stripes and oscillating regions or may settle into a static stripe phase or a oscillating homogeneous state. (The smaller the system the broader the range of ℓ on which one finds mixed states.) The lifetime of transient can vary by one order of magnitude with different initial conditions and is rapidly increasing function of system size.

A quantitative measure of the persistence time is the time required for the system to evolve to a state in which $\phi_{i,j}$ is the same sign for all i, j. Defining $\ln\tau = \langle \ln\tau \rangle$, where $\langle\,\rangle$ indicates the average over the initial conditions, we find that for $r_0 = 0.03$ and $\ell = 0.5$, $\tau \approx 2700$ for $L_x = L_y = 160$, $\tau \approx 650$ for $L_x = L_y = 80$, and $\tau \approx 170$ for $L_x = L_y = 40$ (the averages are over 30–80 initial conditions). The lifetime of transient state grows rapidly with system size and is consistent with diffusion being the dominant process since $\tau \sim L_x^2$. For infinite systems the transient state may persist indefinitely. [Note that we have taken the average of the $\ln(\tau)$ rather than τ itself so that rare long-lived states do not dominate the average.]

Figure 10 shows the value of ℓ at which the transition from stripes to oscillating homogeneous states occur as a function of r_0. We find ℓ_1^* and ℓ_2^* such that for all $\ell < \ell_1^*$ the asymptotic state is a homogeneous oscillating state and for all $\ell > \ell_2^*$ the asymptotic state is a disordered stripe phase. In this way we can bracket the transition to within a narrow band of ℓ. In addition to ℓ^* decreasing with r_0/D we also find that the period of the oscillations decreases rapidly with r_0/D. For example, for $r_0/D = 0.03$ the period is about 50 and for $r_0/D = 0.003\,75$ the period is about 500.

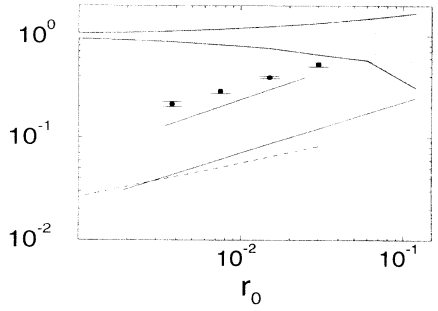

FIG. 10. The value of ℓ at which the transition from stripe phase to oscillating homogeneous phase occurs as a function of r_0. The error bars indicate the bracketed region as explained in the text. The shaded area is where the linear stability analysis predicts oscillatory behavior. The solid line is the value of ℓ at which the simultaneous Eckhaus-zigzag instability occurs obtained from the weak segregation limit and the dashed line is that value obtained from the strong segregation limit. A line proportional to $r_0^{1/2}$ is drawn as a guide to the eye.

One possible reason for the oscillatory behavior is that the linear dispersion relation [Eq. (4.1)] predicts an oscillatory instability. The linear stability analysis predicts a complex ω_k for $k = 0$, if $1 - 2\sqrt{r_0} < \ell < 1 + 2\sqrt{r_0}$ and that ω_k to be unstable if $\ell < 1$. The band with complex ω_k is also shown in Fig. 10. It is clear that we can rule out the oscillatory linear dynamics as the reason for the oscillatory asymptotic state. In fact, except near onset, we do not see any reflection of the linear behavior in the final state. For example, we do not see any qualitative differences as we cross $\ell = 1$ even though this is an important boundary in the linear analysis as the $k = 0$ mode is unstable for $\ell < 1$ and stable for $\ell > 1$.

We also plot the values of ℓ at which the simultaneous Eckhaus-zigzag instability occurs. Our data are primarily for the weak segregation case in which $\ell^* \sim (r_0/D)^{1/2}$. We find that the ℓ for the Eckhaus-zigzag instability is approximately a factor of 4 smaller than ℓ^*, the value of ℓ at which the transition occurs in our numerical experiment. However, the scaling behavior seems to agree in this range of parameters and the result is consistent with the requirement that ℓ^* is larger than that predicted by this instability.

VI. SUMMARY

To summarize, we have introduced a continuum model of laser induced melting. In this model, the presence of

coexisting solid-liquid regions within the illuminated area is due to the higher reflectivity of the molten regions. We showed that, in the limit of large latent heat, the dynamics becomes equivalent to a model of block copolymers [12,11,22]. In particular, any static state of the laser induced melting model is also a static state of the block copolymer model. As the latter is based on an equilibrium free energy this analogy can be used to obtain the wave number of the patterns observed in the laser induced melting experiments. Via this analogy we justified the approximate free energy argument of Hawkins and Biegelsen [2].

We also derived the phase diffusion equations describing the slowly varying stripes. The selected wave number k of the patterns is the one in which the tangential diffusion constant $D_s(k)$ vanishes, i.e., the wave number marginally stable to slow variations in the orientation (the zigzag instability). Therefore the wave number of the lamellae is also given by the stability criteria. We obtained this wave number via systematic expansions from two limits, near onset (weak segregation) and far from onset (strong segregation). The wave number is in good agreement with experiment corresponding to the strong segregation limit [6]. These are very general results for a wide class of systems. In particular, we argue that the vanishing of the tangential diffusion constant at the selected wave number is the reason that the length scale on which regions are orientationally correlated grow as $t^{1/4}$ in simulations of quenches of the Swift-Hohenberg equation [19].

We also discussed a new instability. The lamellae can become unstable to the zigzag instability and Eckhaus instability (slow variations in the wave number) simultaneously. We conjecture that this instability is a signal of time-dependent asymptotic states which are observed experimentally.

We numerically study the behavior after a quench. We find strong agreement between our analytic prediction for the selected wave number and the numerical simulation results as indicated by the peak in the scattering intensity. There are two qualitatively different types of patterns determined by the distance (in parameter space) from onset. Near onset, locally parallel stripes slowly straighten out in time. Far from onset, a disordered lamellar structure is formed in which the lamellae bend on the same length scale as the characteristic lamellar width. This qualitative difference is also reflected in the scattering intensity.

To study this behavior further, we constructed the director field and measure the orientational correlation length. Close to onset, the behavior of the orientational correlation length is consistent with a $t^{1/4}$ growth with the final length being of the order of the system size. Further from onset the correlation length quickly saturates. The product of the orientational correlation length and the selected wave number approaches a limit with decreasing r_0/D (i.e., far from onset). Based on our data and the conclusions of a simulation of the Swift-Hohenberg equation by Elder *et al.* [19], we conjecture that there may be a dynamical phase transition dividing a regime near onset where the orientational correlation length grows until limited by the system size and a second regime in which the orientational correlation length saturates at a value which depends on the distance from onset. Much more extensive numerical work will be required to demonstrate whether this conjecture is true.

Finally we studied dynamics for smaller latent heat in which the system may evolve to a time-dependent asymptotic state. In this case we observe a long-lived transient state which eventually evolves into a homogeneous oscillating state. The persistence time of the transient state depends on the system size. We sketch out the boundary between this and the regime in which the static steady state is reached as a function of latent heat ℓ and reflectivity difference r_0. We find that the value of ℓ at which this transition occurs is larger than that predicted by the simultaneous Eckhaus-zigzag instability. However, the scaling behavior for the phase boundary agrees with that of this instability. This indicates that this instability marks the limit of metastability of the locally parallel stripes.

ACKNOWLEDGMENTS

We are grateful to H. van Driel, D. Kurtze, C. Sagui, T. R. Rogers, and Y. Oono for helpful comments and discussions. We are grateful to D. Jasnow for allowing us to clog his computer workstation. This work was supported by the Natural Sciences and Engineering Research Council of Canada.

APPENDIX A: STATIC SOLUTIONS

In this appendix we show that the static solutions can be obtained via systematic expansions around the small amplitude and sharp interface limits. Assuming periodic stripes of wave number k and the normal in the x direction, the one-dimensional static solution obeys

$$0 = \partial_x^2 \left[\mu_B(\phi) + \partial_x^2 \phi\right] - B\phi. \tag{A1}$$

The reduced temperature field u can be obtained using the relation $\partial_x^2 u = r_0\,\phi/D$.

1. Sharp interfacial limit

For small B, we break up the system into four sections consisting of two outer (bulk) regions corresponding to the positive and negative ϕ phases and two inner regions consisting skin of thickness unity around the two interfaces. In the outer regions we are interested in length scales of order $\lambda \sim k^{-1}$. We introduce the small parameter $\epsilon = \lambda^{-1}$. To extract the large distance behavior, we rescale the normal direction by $X = \epsilon x$ in the outer region. The interfacial width is order unity so the normal direction is not rescaled in the inner region. B must also be rescaled since it determines the pattern wave number. In the bulk phases $\phi = \pm 1$, as $B \to 0$. Using this condition in Eq. (A1) gives $B = \mathcal{O}(\epsilon^3)$. Therefore we rescale

B by $\tilde{B} = \epsilon^{-3}B$.

In the outer regions the static solution obeys

$$0 = \partial_X^2 \mu(\phi) - \epsilon \tilde{B}\, \phi, \tag{A2}$$

where $\mu(\phi) = \mu_B(\phi) + \epsilon^2 \partial_X^2 \phi$. In the inner region the static solution is given by

$$0 = \partial_x^2 \mu(\phi) - \epsilon^3 \tilde{B}\, \phi, \tag{A3}$$

where $\mu(\phi) = \mu_B(\phi) + \partial_x^2 \phi$. In each region we expand $\phi = \phi_0 + \epsilon\phi_1 + \mathcal{O}(\epsilon^2)$ and $\mu(\phi) = \mu_0 + \epsilon\mu_1 + \mathcal{O}(\epsilon^2)$. The matching conditions for μ at the boundary between inner and outer domains are $\phi_i^{\text{inner}} = \phi_i^{\text{outer}}$ and $\partial_x^m \phi_{i+m}^{\text{inner}} = \partial_X^m \phi_i^{\text{outer}}$.

The inner equation gives

$$\phi(x) = \phi_0(x) + \mathcal{O}(\epsilon^2), \tag{A4}$$

where ϕ_0 is the planar interfacial profile for $B = 0$. (We have used the condition that $\phi_{i>0}$ is orthogonal to the Goldstone translation mode $d\phi_0/dx$.) The outer equation gives

$$\phi(X) = \pm\left[1 + \epsilon\chi\tilde{B}X\left(X \mp \frac{1}{2}\right)\right] + \mathcal{O}(\epsilon^2), \tag{A5}$$

where $\chi^{-1} = d\mu_B/d\phi|_{\phi=1}$ and $X = x/\lambda$. For $\mu_B = -\phi + \phi^3$ and $\chi = 1/2$. In the outer region the temperature field becomes

$$u(X) = \pm\left[\epsilon\frac{\tilde{B}}{2}X\left(X \mp \frac{1}{2}\right) + \epsilon^2\chi\tilde{B}^2\frac{X}{12}\left(X^2(X \mp 1) \pm \frac{1}{8}\right)\right] + \mathcal{O}(\epsilon^3). \tag{A6}$$

In the inner region $u(x) = \mathcal{O}(\epsilon^3)$.

2. Weak segregation limit

In the weak segregation limit we use standard methods [21] to expand the solution around the critical point $B = B_0 = 1/4$, $k = k_0 = 1/\sqrt{2}$. We define a small parameter ϵ defined by $B_0 - B = \epsilon^2$ and assume $k = k_0 + \epsilon k_1$. The static solution obeys

$$0 = -\partial_x^2\left(\phi - \phi^3 + \partial_x^2\phi\right) - (B_0 - \epsilon^2)\phi, \tag{A7}$$

where we have used $\mu_B = -\phi + \phi^3$. We want a solution for wavelength $\lambda = 2\pi/k$. We can write the solution as

$$\phi(x) = \sum_{m=1}^{\infty} \epsilon^m f_m(kx), \tag{A8}$$

where $f_m(\theta) = f_m(\theta + 2\pi)$. To fix the position of the interface, we require that f_m be orthogonal to f_m'. We can now write Eq. (A7) order by order in ϵ. First order gives

$$0 = \mathcal{L}_0 f_1(\theta), \tag{A9}$$

where $\mathcal{L}_0 = -\left(k_0^2\partial_\theta^2 + k_0^4\partial_\theta^4 + B_0\right)$. This gives $f_1(\theta) = A_k \sin(\theta)$. (We assume odd symmetry.) The second order expression along with the orthogonality condition gives $f_2 = 0$. The third order condition is

$$-\mathcal{L}_0 f_3 = -\left(k_1^2\partial_\theta^2 + 6k_1^2k_0^2\partial_\theta^4 - 1\right) f_1 + k_0^2\partial_\theta^2 f_1^3. \tag{A10}$$

The solvability condition requires that the right-hand side is orthogonal to the zero eigenvector of $\mathcal{L}_0$, which is simply $\sin(\theta)$. Applying this condition gives

$$\frac{3}{8}A_k^3 = k_1^2 A_k - 6k_1^2k_0^2 A_k + A_k = (1 - 2k_1^2)A_k, \tag{A11}$$

or $A_k^2 = 8(1 - 2k_1^2)/3$. Substituting this into Eq. (A10) and solving the resulting ordinary differential equation gives $f_3(\theta) = A_{3k}\sin(3\theta)$ with $A_{3k} = 9A_k^3/128$. The next order expression gives $f_4(\theta) = 0$. Therefore the static solution is given by

$$\phi(x) = \epsilon A_k \sin(kx) + \epsilon^3 A_{3k}\sin(3kx) + \mathcal{O}(\epsilon^5) \tag{A12}$$

and

$$u(x) = \epsilon\frac{A_k}{k^2}\sin(kx) + \epsilon^3\frac{A_{3k}}{9k^2}\sin(3kx) + \mathcal{O}(\epsilon^5). \tag{A13}$$

APPENDIX B: PHASE DIFFUSION EQUATIONS

1. Rescaled variables and separation of length scales

In this appendix we derive the phase diffusion description of the laser induced melting model. Our derivation closely follows the derivation of Cross for convection models [20].

We assume that the system consists of stripes with slowly varying wave number and orientation. There are two relevant length scales: first, the wavelength of the patterns and second, the length scale on which the orientation and wave number varies. We are interested in the behavior on this second large length and long time scales. In order to separate the two length scales we introduced the slow variables

$$\mathbf{X} = \epsilon\mathbf{r}, \quad T = \epsilon^2 t, \tag{B1}$$

where ϵ is a small parameter and the rapidly varying phase variable $\theta(\mathbf{r}, t)$. This mixture of slow and fast variables is somewhat cumbersome so we introduce a slow phase $\Theta = \epsilon\theta$. The local wave vector $\mathbf{k}$ of the stripes is

$$\boldsymbol{\nabla}\theta(\mathbf{r}, t) = \boldsymbol{\nabla}_{\mathbf{X}}\Theta(\mathbf{r}, t) = \mathbf{k}(\mathbf{X}, T). \tag{B2}$$

The dynamical fields are of the form

$$\phi(\mathbf{r}, t) = \phi(\theta(\mathbf{r}, t), \mathbf{X}, T), \quad u(\mathbf{r}, t) = u(\theta(\mathbf{r}, t), \mathbf{X}, T), \tag{B3}$$

where ϕ and u are 2π periodic function of θ whose functional form depends on the local wave number k.

In the new coordinate systems, the gradient becomes $\boldsymbol{\nabla} = \mathbf{k}\partial_\theta + \epsilon\boldsymbol{\nabla}_{\mathbf{X}}$. The Laplacian is

$$\nabla^2 = k^2\partial_\theta^2 + \epsilon D_1 \partial_\theta + \epsilon^2 D_2, \tag{B4}$$

where D_1 and D_2 depends only on the slow variables $\mathbf{X}, T$, with

$$D_1 = 2k^2\partial_W + k\frac{\partial k}{\partial W} + k\mathcal{K}_W \tag{B5}$$

and

$$D_2 = k\mathcal{K}_W\partial_W + \ell\mathcal{K}_S\partial_S + (k\partial_W)^2 + (\ell\partial_S)^2. \tag{B6}$$

Here W is the rescaled distance in the normal direction with $\hat{\mathbf{W}}\cdot\boldsymbol{\nabla}_{\mathbf{X}} = k\partial_W$ and S is the rescaled distance in the tangential direction with $\hat{\mathbf{S}}\cdot\boldsymbol{\nabla}_{\mathbf{X}} = \ell\partial_S$. $\mathcal{K}_W = \boldsymbol{\nabla}_{\mathbf{X}}\cdot\hat{\mathbf{w}}$ is the curvature of the W =const contours and $\mathcal{K}_S = \boldsymbol{\nabla}_{\mathbf{X}}\cdot\hat{\mathbf{s}}$ is the curvature of the S =const contours. The time derivative is

$$\partial_t = \frac{\partial\theta}{\partial t}\partial_\theta + \epsilon^2\partial_T = \epsilon\frac{\partial\Theta}{\partial T}\partial_\theta + \epsilon^2\partial_T.$$

We expand ϕ and u in orders of ϵ as

$$\phi = \phi_0 + \epsilon\phi_1 + \mathcal{O}(\epsilon^2), \quad u = u_0 + \epsilon u_1 + \mathcal{O}(\epsilon^2). \tag{B7}$$

We can now write the dynamical equations order by order in ϵ.

2. Zeroth-order equations

The zeroth order equations are

$$\begin{aligned} 0 &= -\mu_B(\phi_0) + k^2\partial_\theta^2\phi_0 + u_0, \\ 0 &= Dk^2\partial_\theta^2 u_0 - r_0\phi_0. \end{aligned} \tag{B8}$$

Therefore we find that ϕ_0 and u_0 correspond to static one-dimensional solutions of the model equations. Since the static solutions exists for a band of wave number k, ϕ_0 and u_0 depend on the slow variables through the local wave number k.

3. First-order equations

The first order equations are

$$0 = \mathcal{L}_0\begin{bmatrix}\phi_1\\ w_1\end{bmatrix} + \mathcal{L}_1\begin{bmatrix}\phi_0\\ w_0\end{bmatrix}, \tag{B9}$$

where

$$\mathcal{L}_0 = \begin{bmatrix} -\frac{\partial\mu}{\partial\phi_0} + k^2\partial_\theta^2 & 1 \\ -r_0 & Dk^2\partial_\theta^2 \end{bmatrix} \tag{B10}$$

and

$$\mathcal{L}_1 = \begin{bmatrix} -\frac{\partial\Theta}{\partial T}\partial_\theta + \left(2k^2\partial_W + k\frac{\partial k}{\partial W} + k\mathcal{K}_W\right)\partial_\theta & 0 \\ -\ell\frac{\partial\Theta}{\partial T}\partial_\theta & -\frac{\partial\Theta}{\partial T}\partial_\theta + D\left(2k^2\partial_W + k\frac{\partial k}{\partial W} + k\mathcal{K}_W\right)\partial_\theta \end{bmatrix}. \tag{B11}$$

We apply the solvability condition $\langle\nu_0\mathcal{L}_1\psi_0\rangle = 0$ where $\psi = (\phi, w)$ and ν_0 are the null eigenmodes of $\mathcal{L}_0$, that is, $\nu_0\mathcal{L}_0 = \mathcal{L}^\dagger\nu_0 = 0$. For $\mathcal{L}_0$ the null eigenmode is

$$\nu_0 = \left(\partial_\theta\phi_0, -\frac{1}{r_0}\partial_\theta w_0\right).$$

The solvability condition gives

$$\begin{aligned} 0 = &\left(-\frac{\partial\Theta}{\partial T} + k^2\partial_W + k\frac{\partial k}{\partial W} + k\mathcal{K}_W\right)\frac{1}{2\pi}\int_0^{2\pi} d\theta\ (\partial_\theta\phi_0)^2 + \frac{\ell}{r_0}\frac{\partial\Theta}{\partial T}\frac{1}{2\pi}\int_0^{2\pi} d\theta\ (\partial_\theta w_0)(\partial_\theta\phi_0) \\ &+ \left(\frac{\partial\Theta}{\partial T} - Dk^2\frac{\partial}{\partial u} - Dk\frac{\partial k}{\partial w} - Dk\mathcal{K}_W\right)\frac{1}{2\pi}\int_0^{2\pi} d\theta\ (\partial_\theta u_0)^2. \end{aligned} \tag{B12}$$

We can introduce the coefficients

$$\begin{aligned} \frac{1}{2\pi}\int_0^{2\pi}\phi_0^2 &= A_\phi(k), \\ \frac{1}{2\pi}\int_0^{2\pi}(\partial_\theta\phi_0)^2 &= A_\phi(k)q_{\phi,k}, \\ \frac{1}{2\pi}\int_0^{2\pi} w_0^2 &= A_u(k), \\ \frac{1}{2\pi}\int_0^{2\pi}(\partial_\theta w_0)^2 &= A_u(k)q_{u,k}. \end{aligned}$$

These coefficients depends only on the static one dimensional solutions ϕ_0 and u_0. Therefore the coefficients depend on the local wave number k. We also have

$$\begin{aligned} \frac{1}{2\pi}\int_0^{2\pi} d\theta\ (\partial_\theta w_0)(\partial_\theta\phi_0) &= -\frac{1}{2\pi}\int_0^{2\pi} d\theta\ \phi_0\,\partial_\theta^2 w_0 \\ &= -\frac{r_0}{Dk^2}\frac{1}{2\pi}\int_0^{2\pi} d\theta\ \phi_0^2 \\ &= -\frac{r_0}{Dk^2}A_\phi(k). \end{aligned} \tag{B13}$$

Note that this implies that $A_u(k) \sim r_0^2/(D^2k^4)$, confirming our intuition that the temperature field mediates an effective long range interaction.

4. Phase diffusion equations and Liapunov functional

The phase diffusion equation is now

$$\left(A^2 q_{\phi,k} + \frac{\ell}{Dk^2} A_\phi(k) - \frac{1}{r_0} A_u(k) q_{u,k}\right) \partial_T \Theta$$

$$= \left[k^2 \partial_W + k \frac{\partial k}{\partial w} + k\mathcal{K}_W\right] \times \left(A_\phi(k) q_{\phi,k} - \frac{D}{r_0} A_u(k) q_{u,k}\right), \tag{B14}$$

which we can write as

$$\tau_k \partial_T \Theta = -\boldsymbol{\nabla}_X \cdot \mathbf{k}\, G(k), \tag{B15}$$

where

$$G(k) = \frac{D}{r_0} A_u(k) q_{u,k} - A_\phi(k) q_{\phi,k} \tag{B16}$$

and

$$\tau_k = \left(A_\phi(k) q_{\phi,k} + \frac{\ell}{Dk^2} A_\phi(k) - \frac{1}{r_0} A_u(k) q_{u,k}\right). \tag{B17}$$

In terms of the original coordinates the phase diffusion equation becomes

$$\begin{aligned} \tau_k \partial_t \theta &= -\boldsymbol{\nabla} \cdot \mathbf{k}\, G(k) \\ &= -G(k) \boldsymbol{\nabla} \cdot \mathbf{k} - k \frac{dG(k)}{dk} \frac{\partial k}{\partial w} \\ &= -\frac{dkG(k)}{dk} \partial_w^2 \theta - G(k) \partial_s^2 \theta, \end{aligned} \tag{B18}$$

where we have used $\mathbf{k} = \boldsymbol{\nabla}\theta$. Therefore, assuming $\tau_k > 0$, the system is stable against variations in the normal direction if $d[kG(k)]/dk < 0$ (the Eckhaus instability) and stable against variations along the tangential direction if $G(k) < 0$.

Now let us show that the selected wavelength is exactly the one marginally stable against the zigzag instability, i.e., $G(k) = 0$. In the absence of defects and boundary effects, we can define a Liapunov function via [20]

$$F\{k(\mathbf{r})\} = -\frac{1}{2} \int d\mathbf{r} \int_0^{k(\mathbf{r})^2} dk'^2\, G(k'). \tag{B19}$$

We can show F is a Liapunov functional via

$$\partial_t F = -\frac{1}{2} \int d\mathbf{r}\, \partial_t k^2\, G(k) = -\int d\mathbf{r}\, \tau_k \left(\partial_t \theta\right)^2. \tag{B20}$$

It is easy to see that this function is minimized when $G(k) = 0$.

5. Sharp interface limit

We now calculate the coefficients in the sharp interface limit. Using the static solutions equations (A5) and (A6) gives

$$\begin{aligned} A_\phi(k) &= 1 + \mathcal{O}(\epsilon), \\ A_\phi(k) q_{\phi,k} &= \frac{1}{\pi k} \bar{\sigma} + \mathcal{O}(\epsilon), \\ A_u(k) &= \left(\frac{r_0}{D}\right)^2 \frac{\pi^4}{120k^4} - \frac{17}{5040} \left(\frac{r_0}{D}\right)^3 \frac{\chi \pi^6}{k^6} + \mathcal{O}(\epsilon^4), \\ A_u(k) q_{u,k} &= \left(\frac{r_0}{D}\right)^2 \frac{\pi^2}{12k^4} - \frac{1}{30} \left(\frac{r_0}{D}\right)^3 \frac{\chi \pi^4}{k^6} + \mathcal{O}(\epsilon^4). \end{aligned} \tag{B21}$$

Note that r_0 is $\mathcal{O}(\epsilon^3)$. This gives

$$G(k) = \frac{r_0}{D} \frac{\pi^2}{12k^4} - \frac{1}{60} \left(\frac{r_0}{D}\right)^2 \frac{\chi \pi^4}{k^6} - \frac{\sigma}{\pi k} + \mathcal{O}(\epsilon). \tag{B22}$$

The leading order result for τ_k is

$$\tau_k = \left(\frac{D-1}{D}\right) \frac{\sigma}{\pi k} + \frac{\ell}{Dk^2} - G(k) + \mathcal{O}(\epsilon). \tag{B23}$$

For $\tau_k > 0$, the stability condition against the zigzag instability is $G(k) < 0$ or $\lambda < \lambda^*$ with

$$\lambda^* = \left(\frac{96 D \bar{\sigma}}{r_0}\right)^{1/3} + \frac{8\chi\bar{\sigma}}{5} + \mathcal{O}(\epsilon). \tag{B24}$$

For $\tau_k > 0$, the stability condition against the Eckhaus instability is $d(kG(k))/dk < 0$ or

$$\frac{dkG(k)}{dk} = -\frac{\pi^2 r_0}{4Dk^4} + \frac{2\pi^6 \chi r_0^2}{3D^2 k^6} + \mathcal{O}(\epsilon) < 0. \tag{B25}$$

Therefore if the lamellae are stable against the zigzag instability, they are also stable to the Eckhaus instability.

6. Weak segregation limit

In the weak segregation limit, we expand in $\epsilon^2 = B_0 - B$. Using the static solution given by Eqs. (A12) and (A13), the coefficients become

$$\begin{aligned} A_\phi(k) &= \frac{\epsilon^2 A_k^2}{2} \left[1 + \epsilon^4 \left(\frac{9}{128}\right)^2 A_k^4\right], \\ A_\phi(k) q_{\phi,k} &= \frac{\epsilon^2 A_k^2}{2} \left[1 + \epsilon^4 \left(\frac{27}{128}\right)^2 A_k^4\right], \\ A_u(k) &= \frac{\epsilon^2 A_k^2}{2} \frac{r_0^2}{D^2 k^4} \left[1 + \epsilon^4 \left(\frac{1}{128}\right)^2 A_k^4\right], \\ A_u(k) q_{u,k} &= \frac{\epsilon^2 A_k^2}{2} \frac{r_0^2}{D^2 k^4} \left[1 + \epsilon^4 \left(\frac{3}{128}\right)^2 A_k^4\right]. \end{aligned} \tag{B26}$$

This gives $G(k)$ as

$$G(k) = \frac{\epsilon^2 A_k^2}{2}\left[1 - \frac{r_0}{Dk^4} + \epsilon^4\left(\frac{3}{128}\right)^2 A_k^4\left(81 - \frac{r_0}{Dk^4}\right)\right]. \tag{B27}$$

The leading order expression for τ_k is

$$\tau_k = \epsilon^2 A_k^2 \frac{r_0}{D}\frac{D-1}{2Dk^4} + \epsilon^2 A_k^2 \frac{\ell}{2Dk^2} - G(k) + \mathcal{O}(\epsilon^6). \tag{B28}$$

APPENDIX C: NUMERICAL DETAILS

In order to numerically update the laser induced melting model we use a Euler discretization. Due to the large mesh size and time step ($\delta x = 1.25$ and $\delta t = 0.2$) the update does not reproduce the partial differential equations in the sense of obtaining the exact position of interfaces. However, the numerical method does reproduce the large scale behavior such as the average pattern length. This is checked qualitatively by varying the mesh sizes and step sizes.

The mesh can produce large anisotropy effects. Oono and Puri reduced the anisotropy by including the next nearest neighbors in the discretized Laplacian [34]. They used for their Laplacian (in two dimensions)

$$\begin{aligned}(\delta x)^2[\nabla^2 u]_{i,j} = \frac{1}{1+2\Delta}\Big[&u_{i+1,j} + u_{i,j+1} + u_{i-1,j} + u_{i,j-1} \\ &+\Delta\,(\,u_{i+1,j+1} + u_{i+1,j-1} \\ &+u_{i-1,j-1} + u_{i+1,j-1}\,) \\ &-4(1+\Delta)u_{i,j}\Big],\end{aligned} \tag{C1}$$

with $\Delta = 1/2$ so that the next nearest neighbors $1/2$ weight relative to the nearest neighbors.

Here we consider different values of Δ. In Fourier representation the discretized Laplacian is

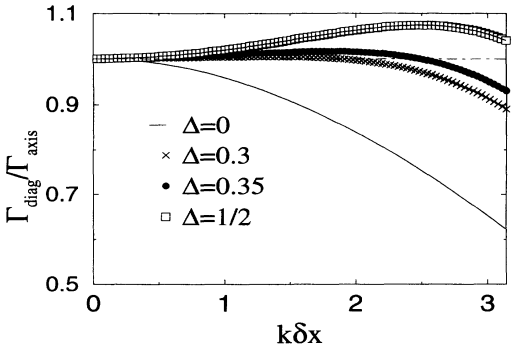

FIG. 11. The ratio of the sphericalized Laplacian in Fourier space along the diagonals divided by its value along the axis. $\Delta = 0$, $\Delta = 0.3$, $\Delta = 0.35$, and $\Delta = 1/2$ are shown.

$$\begin{aligned}(\delta x)^2\,\Gamma(\mathbf{k}) = \frac{2}{1+2\Delta}\Big(&1 - \cos(k_x\delta x) + 1 - \cos(k_y\delta x) \\ &+\Delta\,\{1 - \cos[(k_x+k_y)\delta x] + 1 \\ &- \cos[(k_x - k_y)\delta x]\}\Big).\end{aligned} \tag{C2}$$

We want to make Γ_k as isotropic as possible. As a measure of the anisotropy we use the ratio of $\Gamma(\mathbf{k})$ at different angles θ where $\mathbf{k} = (k\cos(\theta), k\sin(\theta))$. Figure 11 shows a plot of the ratio $\Gamma(k/\sqrt{2}, k/\sqrt{2})/\Gamma(k,0)$ for $\Delta = 0, 0.3, 0.35$, and $1/2$. For all values of Δ, this ratio approaches unity in the limit $k\delta x \to 0$. For small $k\delta x$, the ratio is larger than one and becomes unity at a value of $k\delta x = (k\delta x)^*$ which increases with increasing Δ. Note that $(k\delta x)^* = 0$ for $\Delta = 0$. From this plot it is clear that the choice of $\Delta = 1/2$ does reduce the anisotropy from $\Delta = 0$. However, $\Delta = 1$ makes Γ on the diagonals too large relative to the axis. For our simulations we choose $\Delta = 0.35$, which seems to give a nice compromise between making the value of Γ on the diagonals too large for small $k\delta x$ and too small for larger $k\delta x$.

[1] M.A. Bösch and R.A. Lemons, Phys. Rev. Lett. **47**, 1151 (1981); R.A. Lemons and M.A. Bösch, Appl. Phys. Lett. **40**, 703 (1982).

[2] W.G. Hawkins and D.K. Biegelsen, Appl. Phys. Lett. **42**, 358 (1983).

[3] R.J. Nemanich, D.K. Biegelsen, and W.G. Hawkins, Phys. Rev. B **27**, 7817 (1983).

[4] J.S. Preston, H.M. van Driel, and J.E. Sipe, Phys. Rev. Lett. **58**, 69 (1987); Phys. Rev. B **40**, 3942 (1989).

[5] K. Dworshak, J.E. Sipe, and H.M. van Driel, J. Opt. Soc. Am. B **7**, 981 (1990).

[6] K.F. Dworschak and H.M. van Driel, Phys. Rev. Lett. **69**, 3487 (1992); K.F. Dworschak, Ph.D. thesis, University of Toronto, 1992.

[7] J.S. Preston, J.E. Sipe, H.M. van Driel, and J. Luscombe, Phys. Rev. B **40**, 3931 (1989).

[8] K.A. Jackson and D.A. Kurtze, J. Cryst. Growth **71**, 385 (1985).

[9] L. Leibler, Macromolecules **13**, 1602 (1980).

[10] T. Ohta and K. Kawasaki, Macromolecules **19**, 2621 (1986).

[11] F. Liu and N. Goldenfeld, Phys. Rev. A **39**, 4805 (1989).

[12] Y. Oono and M. Bahiana, Phys. Rev. Lett. **61**, 1109 (1988).

[13] R.E. Rosenweig, M. Zahn, and R. Shumovich, J. Magn. Magn. Mater. **39**, 127 (1983).

[14] P. Molho, J. Gouzerh, J.C.S. Levy, and J.L. Porteseil, J. Magn. Magn. Mater. **54-57**, 857 (1986).

[15] M. Seul and C.A. Murray (unpublished).

[16] C. Roland and R.C. Desai, Phys. Rev. B 42, 6658 (1990); C. Sagui and R. C. Desai, Phys. Rev. Lett. **71**, 3995 (1993).

[17] See, for example, C. Normand, Y. Pomeau, and M. Verlarde, Rev. Mod. Phys. **49**, 581 (1977); F.H. Busse, Rep. Prog. Phys. **41**, 1929 (1978).

[18] J. Toner and D. Nelson, Phys. Rev. **23**, 316 (1981).

[19] K. Elder, J. Viñals, and M. Grant, Phys. Rev. Lett. **68**, 3024 (1992); Phys. Rev. B **46**, 7618 (1992).
[20] M.C. Cross and A.C. Newell, Physica **10D**, 299 (1984).
[21] See, for example, J. Manneville, *Dissipative Structures and Weak Turbulence* (Academic, New York, 1990).
[22] M. Bahiana and Y. Oono, Phys. Rev. A **41**, 6763 (1990).
[23] J.B. Collins and H. Levine, Phys. Rev. B **31**, 6119 (1985); G. Caginalp, Phys. Rev. A **39**, 5887 (1993).
[24] (a) T. Hashimoto, M. Shibayama, and H. Kawai, Macromolecules **13**, 1237 (1980); (b) A. Chakrabarti and J. D. Gunton, Phys. Rev. E **47**, 792 (1993).
[25] (a) Y. Pomeau and J. Manneville, J. Phys.(Paris) Lett. **40**, L609 (1979); (b) K. Kawasaki and T. Ohta, Physica A **139**, 223 (1986).
[26] F.H. Busse and R.H. Clever, J. Fluid. Mech. **91**, 319 (1979).
[27] J.P. Gollub and J.F Steinman, Phys. Rev. Lett. **47**, 505 (1981)
[28] H.S. Greenside and M.C. Cross, Phys. Rev. A **31**, 2992 (1985).
[29] W.W. Mullins and R.F. Sekerka, J. Appl. Phys. **35**, 444 (1964).
[30] P. Manneville, J. Phys. (Paris) **44**, 563 (1983).
[31] H.S. Greenside and W.M. Coughran, Phys. Rev. A **30**, 398 (1984).
[32] J. Swift and P.C. Hohenberg, Phys. Rev. A **15**, 319 (1977).
[33] M.C. Cross, Phys. Rev. A **25**, 1065 (1982).
[34] Y. Oono and S. Puri, Phys. Rev. Lett. **58**, 836 (1988).

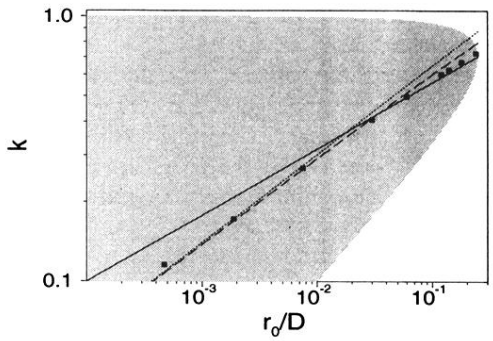

FIG. 2. Graphical summary of the stability analysis. The homogeneous state is linearly unstable within the shaded area. The solid line is $k^* = (r_0/D)^{1/4}$, i.e., the lowest order result for the selected wave number obtained near onset. The dotted line is the lowest order wave number far from onset $k^* = 2\pi(96D\bar{\sigma}/r_0)^{-1/3}$. The dashed line is the far from onset result including next order corrections. The squares are the length scale obtained from simulations with $\ell = 2$ and $D = 0.5$.

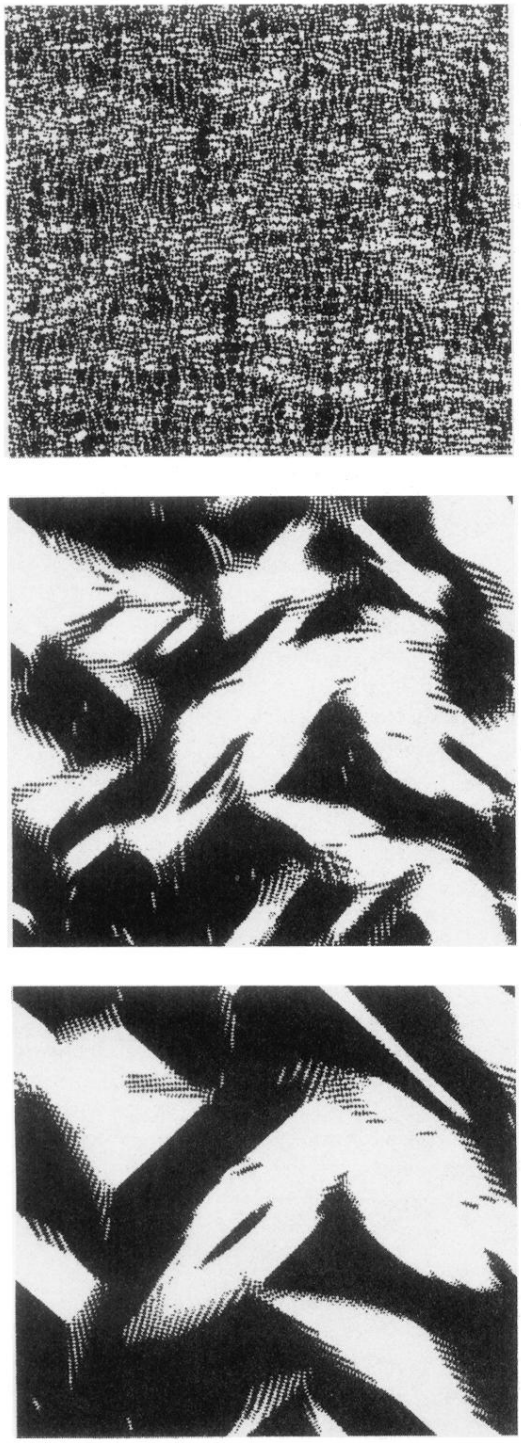

FIG. 6. The director field for $r_0/D = 0.24$ corresponding to the same times as in Fig. 1 ($t = 1600, 12\,800$, and $102\,400$.). The entire 512×512 lattice is shown. The lower left quarter box corresponds to the 256×256 region shown in Fig. 1. White denotes regions with $\cos(2\theta) > 0$ $(-\pi/2 < 2\theta < \pi/2)$ and black denotes $\cos(2\theta) < 0$.